NACA RM E58D28

NACA

RESEARCH MEMORANDUM

EFFECT OF DESIGN VARIABLES ON PERFORMANCE OF MACH 4.0 HYDROGEN EXPANSION ENGINES

By James F. Dugan, Jr.

Lewis Flight Propulsion Laboratory
Cleveland, Ohio

NATIONAL ADVISORY COMMITTEE
FOR AERONAUTICS
WASHINGTON
July 22, 1958

NATIONAL ADVISORY COMMITTEE FOR AERONAUTICS

RESEARCH MEMORANDUM

EFFECT OF DESIGN VARIABLES ON PERFORMANCE OF MACH 4.0 HYDROGEN EXPANSION ENGINES*

By James F. Dugan, Jr.

SUMMARY

Performance calculations were made for hypothetical hydrogen expansion engines in which only a small part of the engine airflow passes through the heat exchanger. The prescribed flight path was representative of those for long-range, high-speed aircraft. The operating mode was set by assigning the operating line on the compressor map and the values for primary-combustor and afterburner temperature.

Performance during acceleration and climb was improved markedly by increasing the number of compressor stages from one to three. The effect on cruise performance was slight. During climb, up to 57 percent higher thrust resulted from the use of completely variable inlets and exits. For the engine having the two-stage compressor, increasing the initial cruise altitude from 85,000 to 105,000 feet increased the minimum specific fuel consumption from 0.848 to 0.879.

INTRODUCTION

The hydrogen expansion engine is one of several powerplants suitable for manned flight at high altitude and high flight Mach numbers. A representative mission might call for cruise at Mach 4.0 and a target altitude of 95,000 feet. In performing such a mission, a hydrogen expansion engine might be superior to other engines because of lower specific fuel consumption and engine specific weight at cruise and higher thrust margins during acceleration and climb.

An evaluation of four powerplants, including several possible configurations of the hydrogen expansion engine, is presented in reference 1 for high-altitude, high Mach number missions. In this reference the hydrogen expansion engine and the air turborocket are shown to yield longer all-supersonic range than the turbojet and turbofan engines.

In order to determine the interrelation of the many engine variables during off-design operation and the effect of design variables on engine performance, several possible hydrogen expansion engines were investigated at the NACA Lewis laboratory. These engines differ from those of reference 1 in that the main body of engine airflow is not required to flow through a heat exchanger. Instead, only a small part of the compressor-exit air is diverted to a fuel-rich combustor whose hydrogen-rich products flow through a heat exchanger. It was hypothesized that this configuration would result in higher engine pressure ratios and smaller, lighter heat exchangers. Off-design engine performance was computed by assigning the operating line on the compressor map and the values of the fuel-rich combustor temperature and the afterburner temperature. Performance calculations were made for engines having one-, two-, and three-stage compressors. The prescribed flight path included acceleration and climb from sea-level takeoff to Mach 4.0 and 70,000 feet, and Mach 4.0 cruise starting at altitudes from 85,000 to 105,000 feet.

ANALYSIS

Functioning of Engine

Tracing the airflow and fuel flow through a schematic diagram of the hydrogen expansion engine (fig. 1) aids in understanding how such an engine functions. The engine airflow, after passing through the inlet (0 to 1), is compressed by a low-pressure-ratio fan (1 to 2). Most of the air then flows through a throttled bypass duct to the afterburner (2 to 7a). A small amount of the fan-exit air, however, enters the primary combustor (5a) and burns fuel-rich with hydrogen (5h). The fuel-rich combustion products pass through the hot side of the heat exchanger (6 to 7) and mix with additional hydrogen and with the main body of bypassed air in the afterburner (7 to 8). Here, final combustion occurs and the hot gases then expand through the exhaust nozzle to produce thrust.

Driving the fan is a small turbine with a working fluid of hydrogen gas. The hydrogen, starting as a liquid in the fuel tank, is pumped to a very high pressure and then used as a heat sink for various cooling requirements. By the time the hydrogen reaches the cold side of the heat exchanger (3), it is a gas. After being heated (3 to 4), the high-pressure high-temperature hydrogen gas is ducted to the turbine that drives the fan through a suitable gear. The hydrogen from the turbine exit is finally injected into the primary combustor (5h).

Components

Inlet. - The all-external-compression inlet employed in the calculations was made up of two cones with half angles of 20° and 35°. Three

percent of the inlet airflow was bled from the throat just inside the cowl lip to remove the boundary layer and improve the turning and velocity profile at the shoulder. The inlet was assumed to be located under a wing so that the flow deflection during cruise would be 0.10 radian. Installation of the inlet under the wing results in higher total-pressure recovery and tends to minimize the effects of variations in pitch angle.

The critical inlet performance shown in figure 2 is for a representative schedule of wing angle of attack with flight Mach number. The vertical part of the total-pressure-recovery curve at Mach 4.0 (fig. 2(a)) results from the change in wing angle of attack in going from Mach 4.0 and 70,000 feet to Mach 4.0 and the initial cruise altitude. In calculating the additive-drag coefficient (fig. 2(e)), some relief from fixed inlet performance was assumed. At Mach 1.5, additive drag was taken as 60 percent of the fixed inlet value. Several schemes might be used to achieve this additive-drag reduction. One of the most promising schemes for the all-external-compression two-cone inlet is translation of the forward cone. Schlieren pictures (unpublished) of an actual inlet operating at Mach 2.0 indicate that separation occurs behind the translated cone. Thus, it is probable that single-cone performance could be obtained at transonic Mach numbers by translating the forward cone of a two-cone inlet. In the present case, the calculated additive-drag coefficient at Mach 1.5 is 40 percent less for the 20° cone than for the 20° plus 35° cones.

Other types of inlets also are suitable for a Mach 4.0 engine. For example, an external-internal-compression inlet employing about 20° of external turning, 10° of external-lip angle, rearward spike translation at transonic Mach numbers, and an efficient bypass system would give pressure recoveries and additive drags similar to the values shown in figure 2.

The inlet performance employed in the calculations (fig. 2) should be obtainable with relatively simple and light-weight inlet designs.

Compressor. - Performance was calculated for hydrogen expansion engines having one-, two-, and three-stage compressors. The one-stage-compressor performance map is based on the one-stage performance presented in reference 2. The two- and three-stage compressor maps were computed by stacking stage performance based on the unpublished performance of a current experimental transonic-inlet stage. Computed performance for the two-stage compressor is shown in figure 3.

Heat exchanger. - Heat-exchanger performance was calculated by using the curves presented in reference 3. The unfinned, staggered, round-tube configuration designated S-2.00-1.00 was used for each engine.

[redacted]

Turbine. - In calculating turbine performance, choked flow through the nozzles and a constant efficiency of 0.70 were assumed for all operating conditions.

Fuel-rich combustor. - The fuel-air ratio was calculated from an equation that equates the energy of the incoming air and hydrogen with the energy of the outgoing stoichiometric products and excess hydrogen. Only momentum losses were considered in calculating pressure ratio across the combustor. The friction losses were assumed to be negligible.

Afterburner. - For all operating conditions, afterburner combustion efficiency was assumed to be 0.95. Momentum total-pressure losses in the afterburner were accounted for by considering the flow from the mixing station (7) to the afterburner exit (8) to be characterized by constant area and constant total momentum. The friction loss was assumed to be equal to the weight-flow-averaged dynamic pressure at station 7.

Exhaust nozzle. - A convergent-divergent ejector-type exhaust nozzle was used. The throat area was variable, while the exit area was fixed. Exhaust-nozzle performance was calculated by assigning a velocity coefficient of 0.975 and by assuming flow separation to occur in the divergent section, where the local static pressure decreased to 70-percent free-stream static pressure. Secondary air would be required to promote separation. More airflow than that bled from the inlet throat and the compressor exit undoubtedly would be required at transonic Mach numbers, but this is not considered in the analysis. In calculating exhaust-nozzle performance for supersonic flight, the average pressure over the separated flow region was approximated by the equation

$$p_{av} = p_0 \frac{1 + \frac{1}{M_0}}{2}$$

(All symbols are defined in appendix A.) For subsonic flight, the exhaust-nozzle thrust coefficient was set equal to 0.975.

The fixed exhaust-nozzle-exit area was calculated for cruise flight conditions with the stipulation that the exit static pressure be 1.7 times the ambient static pressure.

Flight Path and Operating Mode

Performance was calculated for the flight path shown in figure 4. Acceleration from Mach 0 to 0.9 occurred at sea level; this was followed by climb at Mach 0.9 from sea level to 36,089 feet. At the tropopause, acceleration was from Mach 0.9 to 2.0. Acceleration and climb passed through Mach 3.0 and 60,000 feet on up to Mach 4.0 and 70,000 feet. Climb at Mach 4.0 went to the initial cruise altitude of 85,000, 95,000, or 105,000 feet.

[redacted]

The operating mode was fixed by assigning the values for combustor and afterburner temperature and by assigning the operating line on the compressor map. For an actual engine, such an operating mode would require scheduled control of four variables in addition to control of the inlet forward cone: turbine fuel flow, afterburner fuel flow, position of throttle in bypass duct, and size of exhaust-nozzle-throat area. For all operating conditions (except as noted in RESULTS AND DISCUSSION), combustor temperature was assigned to be 2500° R. During acceleration and climb, afterburner temperature was assigned to be 4000° R. For cruise operation, a range of afterburner temperatures from 3000° to 4000° R was considered. The compressor operating line was assigned with due regard to a number of considerations. Compressor weight flow at each flight condition was such that the inlet operated at its critical flow condition. A second compressor variable, compressor total-pressure ratio, was assigned to achieve high total-pressure ratio, good efficiency, adequate surge margin, and acceptable mechanical speed. An additional consideration affecting the selection of compressor total-pressure ratio was the requirement that turbine fuel flow be less than the total fuel flow required for the assigned afterburner temperature. The operating line on the two-stage compressor map is shown in figure 3.

Matching of Components

A detailed description of the steps used in matching the components and calculating engine performance is presented in appendixes B and C. In this section and the one following, the component matching and the performance calculation are outlined. The state of the air entering the engine is found for the specified flight Mach number, altitude, and inlet. All quantities relating to the compressor are set by the assigned compressor operating point. A rather long iteration commences when a trial value of turbine-inlet temperature is set. From this point on, all values are temporary until the iteration loop is closed. Next, the parameters related to the hydrogen turbine are calculated; this includes the fuel flow through the turbine and its pressure and temperature on entering the fuel-rich combustor.

The assigned combustor temperature permits the quantity and state of the fuel-rich combustion products entering the hot side of the heat exchanger to be calculated. From the performance curves of the heat exchanger, a value of turbine-inlet temperature (heat-exchanger cold-side exit temperature) can be calculated. If the calculated value does not equal the trial value, the iteration is repeated until the two values do agree.

The pressure of the fuel-rich gas at the mixing station results from calculating the total-pressure ratios across the combustor and the hot side of the heat exchanger. The required total pressure of the bypassed

[redacted]

air downstream of the bypass throttle is calculated from the condition that the static pressures of the two streams at the mixing station are the same. Approximating the flow from the mixing station to the afterburner exit by a constant-area constant-total-momentum process permits the total pressure at the exhaust-nozzle inlet to be calculated. The fuel-air ratio and the total temperature of the gas at the exhaust-nozzle are calculated from the assigned values of afterburner temperature and efficiency. Sonic velocity at the throat, weight flow, and state of the gas entering the exhaust nozzle permit the calculation of the exhaust-nozzle-throat area.

Performance Calculation

The component matching calculations yielded the following quantities needed to calculate engine performance: inlet weight flow, compressor-exit-bleed weight flow, exit weight flow, total fuel flow, exhaust-nozzle-throat area, exhaust-nozzle pressure ratio, and compressor-exit total temperature and total pressure. The ideal jet velocity was calculated from the gas properties at the nozzle inlet and from ambient pressure. The contribution to thrust from the compressor-exit-bleed air was calculated from the state of the air at the compressor exit. Inlet, nacelle, and exhaust-nozzle performance curves yielded the coefficients to complete the calculation of the engine performance parameters $C_F M_0^2$ and sfc.

RESULTS AND DISCUSSION

The design constants employed in the calculations for the hydrogen expansion engines having one-, two-, and three-stage compressors are listed in table I. Because the trends calculated for the off-design operation of each engine are similar, only the engine having the two-stage compressor is discussed in the following section.

Off-Design Operation

For the assigned flight path (fig. 4) and the assigned operating line on the two-stage compressor map (fig. 3), compressor mechanical speed varies with flight Mach number as shown in figure 5. Maximum speed occurs at Mach 0.9 and sea level, where a value 8 percent higher than for takeoff occurs. For a super alloy steel, the limiting compressor stress condition, however, is at Mach 4.0 cruise, where speed is 87.5 percent of the takeoff value and stagnation-air temperature is 1667° R.

Maximum fan power for the assigned flight path occurs at Mach 0.9 and sea level (fig. 6). By adjusting the flight path, a reduction in

[redacted]

gear weight could be realized. For example, the compressor power at Mach 0.5 and sea level is 33 percent less than that at Mach 0.9 and sea level. A gear-box weight savings of the same order, then, would result by starting climb at Mach 0.5 and specifying an altitude of 39,000 feet at Mach 2.0 instead of 36,000 feet.

Fuel-flow requirements are shown in figure 7. The solid-line curve represents the total fuel flow required to achieve an afterburner temperature of 4000° R. The dashed-line curve is the fuel flow through the turbine compatible with a primary-combustor temperature of 2500° R. At some flight conditions, for example, Mach 0.9 at sea level and Mach 4.0 at 70,000 feet, turbine fuel flow is seen to exceed the total fuel flow. One way of alleviating this unacceptable operating condition is to raise the combustor temperature. In this case, acceptable turbine fuel flows result when combustor temperature is raised to 3000° R. Compromises of this nature are tempered by possible engine-weight penalties.

Turbine-inlet temperature varies between 1200° and 1820° R (fig. 8). The variation shown is for a combustor temperature of 2500° R except for Mach 0.9 at sea level and for Mach 4.0 at 70,000 feet and cruise, where a 3000° R combustor temperature was specified to limit turbine fuel flow. If it is deemed desirable to lower the maximum turbine-inlet temperature, this can be done (still maintaining acceptable turbine fuel flow) by lowering both the combustor temperature and the compressor pressure ratio. Along with decreased compressor pressure ratio, however, would go lower thrust and higher specific fuel consumption.

Turbine equivalent speed was found to vary between 79 and 107 percent of the sea-level takeoff value. This variation in equivalent speed along with the variation in turbine total-pressure ratio (fig. 8) indicates that turbine operation approaching the limiting loading condition would not be encountered. Turbine-inlet pressure varies as shown in figure 9.

The maximum total-pressure loss in the primary combustor is 3.3 percent. Combustor frontal area is 0.6 fan frontal area (table I), so that combustor-inlet Mach numbers range from 0.02 to 0.06.

Through the hot side of the heat exchanger, maximum total-pressure loss is 5.8 percent. Inlet Mach numbers range from 0.04 to 0.19. To achieve these low Mach numbers, a heat-exchanger hot-side free-flow area of 0.73 fan frontal area is required. For the selected core configuration, this requires a heat-exchanger frontal area of 1.77 fan frontal area.

The losses in the combustor and the hot side of the heat exchanger necessitate a total-pressure loss across the throttle in the bypass duct, as shown in figure 10. This loss variation is consistent with the constant static-pressure mixing of the bypassed air and the fuel-rich gas from the heat exchanger.

[redacted]

The total-pressure ratio from the exhaust-nozzle inlet to the fan exit varies between 0.99 at cruise and 0.90 at Mach 0.9 and sea level (fig. 11). This variation is for an afterburner area of 4.06 times the fan frontal area and a flow area for the fuel-rich gases at the mixing station of 1.46 times the fan frontal area.

The total-pressure losses in the engine are dependent on the size of the afterburner and the flow areas at the mixing station allotted to the air and fuel-rich gas streams. Their effect on the exhaust-nozzle-inlet to fan-exit total-pressure ratio is shown in figure 12 for sea-level takeoff operation. For a one "q" (dynamic head) friction loss, the flow-area division has little effect on the total-pressure ratio. As the afterburner frontal area increases from 2 to 4 times the fan frontal area, the total-pressure ratio increases from 0.875 to 0.924. For a two "q" friction loss, the flow-area division does have an effect on the total-pressure ratio. At an afterburner frontal area equal to 2.13 times the fan frontal area, the total-pressure ratio increases from 0.830 to 0.868 as the flow area allotted to the bypass stream increases from 0.67 to 1.40 times the fan frontal area. A bypass flow area less than 0.67 times the fan frontal area is impractical since it would require a total-pressure rise in the bypass duct. The trends shown in figure 12 for Mach 0 and sea level prevail at the other flight conditions. As noted in figure 11, the largest pressure losses occur during subsonic sea-level operation.

Engine Performance

Acceleration and climb. - The effect of compressor pressure ratio on engine performance during acceleration and climb is shown in figure 13. At the lower flight Mach numbers, thrust increases markedly with compressor pressure ratio (fig. 13(a)). At sea-level takeoff, thrust increases 70 percent in going from a one-stage to a three-stage compressor. The improvement is 37 percent at Mach 1.5, where thrust margins might be quite low. The effect of compressor pressure ratio on engine thrust decreases as flight Mach number increases. At Mach 4.0, thrust of the three engines is the same (fig. 13(b)). The favorable effect of compressor pressure ratio on specific fuel consumption (fig. 13(c)) is similar to the effect on thrust.

Also plotted in figures 13(a), (b), and (c) is the performance of a hydrogen-fueled turbojet engine having a three-stage compressor. Flight path, afterburner temperature, inlet performance, and exhaust-nozzle performance are the same as for the hydrogen expansion engines. All during acceleration and climb, the performance of the hydrogen expansion engines is seen to be superior.

In figure 13(d) is plotted the thrust of the hydrogen expansion engine with the two-stage compressor relative to the thrust of the turbojet engine with the three-stage compressor. For a complete comparison, factors other than thrust must be considered, such as engine weight, control complexity, and engine development. These considerations are outside the scope of the analysis, but it seems probable that the turbojet engine would be lighter, less complex, and easier to develop.

Figure 14 shows the improvement in performance during acceleration and climb that results from using a completely variable inlet and exhaust nozzle. Use of the completely variable inlet reduces the maximum-additive-drag coefficient from 0.320 to 0.076. The completely variable exhaust nozzle results in a nozzle thrust coefficient of 0.975 for all operating conditions. Improvement is shown for the hydrogen expansion engine with the two-stage compressor and for the turbojet engine with the three-stage compressor. Maximum improvement, which occurs at Mach 1.6, is 57 percent for the hydrogen expansion engine and 79 percent for the turbojet engine. In the transonic region, then, use of completely variable components would decrease the difference between the hydrogen expansion and turbojet performance. At Mach 1.6, for example, the thrust ratio would decrease from 1.34 to 1.18. Any improvement in inlet and exhaust-nozzle technology would also decrease the performance differences between the two engine types. Use of a completely variable inlet and exhaust nozzle would result in additional control complexity and large weight penalties to offset the improved performance.

Cruise. - Cruise performance of the three hydrogen expansion engines is very similar (figs. 15(a), (b), and (c)). Thrust at cruise increases with increasing afterburner temperature and decreasing altitude. The lower ambient temperature (lower flight velocity) at the lower altitudes accounts for the higher thrust and also for the lower specific fuel consumption. At a given altitude, specific fuel consumption sfc tends to minimize at a particular value of afterburner temperature. This occurs because sfc varies directly with fuel-air ratio and inversely with jet velocity, both of which increase with afterburner temperature. Minimum sfc for the three hydrogen expansion engines occurs at 85,000 feet and ranges from 0.840 to 0.848. For the hydrogen expansion engine with the two-stage compressor, minimum sfc increases from 0.848 at 85,000 feet to 0.879 at 105,000 feet.

The minimum sfc values for the hydrogen expansion engines (figs. 15(a), (b), and (c)) is about 6 percent lower than that for the turbojet engine (fig. 15(d)). The difference is due to the higher engine total-pressure ratio of the hydrogen expansion engine.

Use of a completely variable inlet and exhaust nozzle has no effect on the cruise performance of the hydrogen expansion and turbojet engines because all inlets and exhaust nozzles were designed for the cruise condition; this is reasonable for engines to be used for long-range missions.

[redacted]

CONCLUDING REMARKS

Design compressor pressure ratio has a marked effect on climb performance but only a slight effect on cruise specific fuel consumption. For a given application, selection of design compressor pressure ratio would depend mainly on the compromise involving thrust margins available during acceleration and climb and engine specific weight at cruise.

Climb performance is improved considerably by the use of variable inlets and exits. At Mach 1.6, thrust increased 57 percent when a completely variable inlet and exit were used for the hydrogen expansion engine having a two-stage compressor.

The increase in cruise specific fuel consumption with initial cruise altitude is exemplified by a minimum-specific-fuel-consumption increase from 0.848 at 85,000 feet to 0.879 at 105,000 feet for the engine with the two-stage compressor.

Lewis Flight Propulsion Laboratory
National Advisory Committee for Aeronautics
Cleveland, Ohio, May 12, 1958

[redacted]

APPENDIX A

SYMBOLS

A	area, sq ft
a	speed of sound, ft/sec
b	ratio of bleed airflow to compressor-inlet airflow
C	coefficient
C_D	drag coefficient based on compressor area
$C_{D,a}$	inlet-additive-drag coefficient based on nacelle-lip area
$C_{D,b}$	bleed-drag coefficient based on nacelle-lip area
$C_{D,c}$	cowl-pressure-drag coefficient based on nacelle-lip area
$C_{D,n}$	nacelle-friction and pressure-drag coefficient based on nacelle-lip area
C_F	thrust coefficient based on compressor area
C_f	exhaust-nozzle thrust coefficient
C_{fr}	friction coefficient based on surface area
c_p	specific heat at constant pressure, Btu/(lb)($^\circ$F)
D_h	hydraulic diameter, ft
f	fuel-air ratio
g	acceleration due to gravity, ft/sec^2
H	total enthalpy, Btu/lb
$\overline{H}$	fuel heating value, Btu/lb
h	heat-transfer coefficient, (Btu/sec)/(sq ft)($^\circ$F)
h_s	static enthalpy, Btu/lb
J	mechanical equivalent of heat, 778.2 ft-lb/Btu
K	constant

[redacted]

k	thermal conductivity, (Btu/hr)/(ft)($^{\circ}$F)
M	Mach number
N	rotational speed, rpm
NTU	number of transfer units (eq. (B27))
P	total pressure, lb/sq ft
Pr	Prandtl number
p	static pressure, lb/sq ft
$\mathscr{P}$	power, hp
q	heat-transfer rate, Btu/sec
q_0	free-stream dynamic pressure, lb/sq ft
R	gas constant, ft/$^{\circ}$R
Re	Reynolds number
S	surface area, sq ft
St	Stanton number
sfc	specific fuel consumption, lb fuel/(hr)(lb thrust)
T	total temperature, $^{\circ}$R
t	static temperature, $^{\circ}$R
U	over-all heat-transfer coefficient, (Btu/sec)/(sq ft)($^{\circ}$F)
V	velocity, ft/sec
w	weight flow, lb/sec
Y	function of γ and M (eq. (B32))
Z	function of γ and M (eq. (B33))
γ	ratio of specific heats
δ	ratio of total pressure to NACA standard sea-level pressure of 2116 lb/sq ft

[redacted]

ε		heat-exchanger effectiveness (eqs. (B26) and (B29))
η		efficiency
θ		ratio of total temperature to NACA standard sea-level temperature of 518.7° R
μ		absolute viscosity, lb/(ft)(hr)
ρ		gas density, slugs/cu ft
φ	$\equiv$	$\int \frac{c_p}{T} dT$, Btu/(lb)(°R)
ψ_h	$\equiv$	$(h - h_a) \frac{1 + f}{f}$, Btu/lb

Subscripts:

AB	afterburner
a	air
av	average
b	bleed
C	compressor
cal	calculated
cl	cooling
d	design
f	fuel
fl	flow
fr	friction
in	inlet
id	ideal
l	lip
max	maximum

[redacted]

min	minimum
sl	sea level
st	stoichiometric
T	turbine
t	total
tr	trial
0	free stream
1,2, . . . 10	engine stations (fig. 1)

[redacted]

APPENDIX B

MATCHING OF COMPONENTS

For the assigned altitude, values of a_0, t_0, and p_0 were read from the ICAO standard atmosphere tables. The value of $T_1 = T_0$ was read from the charts of reference 4 after H_0 was calculated from

$$H_0 = h_{s,0} + \frac{M_0^2 \gamma_0 R_a t_0}{2J} \tag{B1}$$

Inlet total pressure P_1 was calculated from

$$P_1 = P_1/P_0 \; (P_0/p_0) \; p_0 \tag{B2}$$

and

$$\frac{P_0}{p_0} = e^{\frac{J}{R_a}(\varphi_{t,0} - \varphi_0)} \tag{B3}$$

where values of φ were read from the charts of reference 4, and P_1/P_0 was read from figure 2.

Compressor parameters were calculated from the assigned compressor operating point and the following equations:

$$w_1 = \left(\frac{w\sqrt{\theta}}{\delta}\right)_1 \frac{\delta_1}{\sqrt{\theta_1}} \tag{B4}$$

$$P_2 = P_2/P_1(P_1) \tag{B5}$$

$$H_2 - H_1 = c_{p,1}(T_2 - T_1) \tag{B6}$$

$$\gamma_1 = \left(\frac{c_p}{c_p - \frac{R}{J}}\right)_1 \tag{B7}$$

$$T_2 - T_1 = \frac{T_1}{\eta_C}\left[(P_2/P_1)^{\frac{\gamma_1 - 1}{\gamma_1}} - 1\right] \tag{B8}$$

[redacted]

Throughout the remainder of the calculation, values of c_p and other parameters that depend on gas composition and temperature were read from the tables of reference 5 or the curves of reference 6.

A trial value of T_4 is selected, and a long iteration begins. For the assigned values of turbine choked flow and efficiency, a value of turbine temperature drop was calculated from the implicit relation

$$T_4 - T_5 = \frac{w_1(H_2 - H_1)\sqrt{T_4}\left(1 - \frac{T_4 - T_5}{T_4\eta_T}\right)^{\frac{\gamma_4}{\gamma_4 - 1}}}{c_{p,4}\left(\frac{w_4\sqrt{T_4}}{P_4}\right)_d P_5} \tag{B9}$$

where P_5, the turbine-outlet total pressure, is assigned to be twice P_2, the compressor-outlet total pressure. This was done to assure proper injection of the hydrogen gas into the primary combustor. Values of turbine fuel flow and total-pressure ratio were calculated from

$$w_4 = \frac{w_1(H_2 - H_1)}{c_{p,4}(T_4 - T_5)} \tag{B10}$$

and

$$\frac{P_5}{P_4} = \left(1 - \frac{T_4 - T_5}{T_4\eta_T}\right)^{\frac{\gamma_4}{\gamma_4 - 1}} \tag{B11}$$

For the primary combustor, which operates fuel-rich, values of fuel-air ratio f_6, airflow $w_{a,6}$, and gas flow w_6 were calculated from:

$$f_6 = \frac{H_{a,5} + 0.02916(H + \overline{H})_{f,6} - 1.02916\, H_{st,6}}{H_{f,6} - H_{f,5}} \tag{B12}$$

$$w_{a,6} = \frac{w_4}{f_6} \tag{B13}$$

$$w_6 = w_4 + w_{a,6} \tag{B14}$$

The value of $\overline{H}$, the heating value of hydrogen, in equation (B12) is 60,194 Btu per pound.

[redacted]

In calculating heat-exchanger performance, gas properties are evaluated for average temperatures. The average cold-side temperature is

$$T_{3-4} = \frac{T_3 + T_4}{2} \tag{B15}$$

where T_3 was assigned to be 300° R for all operating conditions, to account for using the fuel as a heat sink for various cooling duties.

Average hot-side temperature is

$$T_{6-7} = T_6 - \frac{q}{2w_6 c_{p,6-7}} \tag{B16}$$

where

$$q = w_4 c_{p,3-4}(T_4 - T_3) \tag{B17}$$

Because $c_{p,6-7}$ in equation (B16) is a function of T_{6-7}, a simple iteration is required. The value of $c_{p,6-7}$ (as well as the values of μ_{6-7} and k_{6-7} to be used later) were read from curves presented in reference 6.

The hot-side heat-transfer coefficient was calculated from

$$h_{6-7} = \frac{w_6 c_{p,6-7}(StPr^{2/3})_{6-7}}{A_{fl,6-7}(Pr^{2/3})_{6-7}} \tag{B18}$$

where $(StPr^{2/3})_{6-7}$ was read from the appropriate curve in reference 3 for the hot-side Reynolds number

$$Re_{6-7} = \frac{3600\ w_6 D_{h,6-7}}{\mu_{6-7} A_{fl,6-7}} \tag{B19}$$

Values for $D_{h,6-7}$ and $A_{fl,6-7}$ are tabulated in reference 3 for numerous heat-exchanger configurations. The values used in the calculation are listed in table I.

The cold-side heat-transfer coefficient was calculated from

$$h_{3-4} = 0.00386 \left(\frac{w_4}{A_{fl,3-4}}\right)^{0.8} \frac{T_{3-4}^{0.133}}{D_{h,3-4}^{0.2}} \tag{B20}$$

[redacted]

which is derived from the heat-transfer equation for flow through tubes,

$$St = 0.023\ (Re)^{-0.2}\ (Pr)^{-2/3} \tag{B21}$$

the approximate relation for viscosity of hydrogen,

$$\mu = 0.0908\ (10^{-6})\ T^{0.666} \tag{B22}$$

and the approximations for hydrogen gas,

$$c_p = 3.5 \tag{B23}$$

$$Pr = 0.74 \tag{B24}$$

The over-all heat-transfer coefficient was calculated from

$$U = \frac{1.0}{\frac{1}{h_{6-7}} + \frac{1}{h_{3-4}\frac{S_{3-4}}{S_{6-7}}}} \tag{B25}$$

in which the resistance across the tube wall is neglected because it is small, compared with the film resistances.

Heat-exchanger effectiveness was read from curves representing the following equation for counterflow heat exchangers (cf. ref. 3)

$$\varepsilon = \frac{1 - e^{-NTU\left[1 - \frac{(wc_p)_{min}}{(wc_p)_{max}}\right]}}{1 - \frac{(wc_p)_{min}}{(wc_p)_{max}} e^{-NTU\left[1 - \frac{(wc_p)_{min}}{(wc_p)_{max}}\right]}} \tag{B26}$$

The values of $(wc_p)_{min}$ and $(wc_p)_{max}$ are the appropriate values of $w_6c_{p,6-7}$ or $w_4c_{p,3-4}$, while the number of transferred units is

$$NTU = \frac{US_{6-7}}{(wc_p)_{min}} \tag{B27}$$

The iteration loop, which began with the selection of a trial value of T_4 to be used in equation (9), is now completed by calculating a value for $T_{4,cal}$

[redacted]

$$T_{4,cal} = T_3 + \frac{q_{cal}}{(wc_p)_{3-4}} \tag{B28}$$

where

$$q_{cal} = \varepsilon\,(wc_p)_{min}\,(T_6 - T_3) \tag{B29}$$

The steps involving equations (B9) through (B29) are repeated until $T_{4,cal}$ equals $T_{4,tr}$.

The total-pressure ratio across the primary combustor was calculated from momentum considerations; friction effects were neglected. The momentum equation for an unobstructed combustor of uniform cross-sectional area

$$\frac{P_6}{P_{5a}} = \frac{(1 + \gamma_{5a}M_{5a}^2)\left(1 + \frac{\gamma_6 - 1}{2}M_6^2\right)^{\frac{\gamma_6}{\gamma_6 - 1}}}{(1 + \gamma_6 M_6^2)\left(1 + \frac{\gamma_{5a} - 1}{2}M_{5a}^2\right)^{\frac{\gamma_{5a}}{\gamma_{5a} - 1}}} \tag{B30}$$

and the continuity equation

$$(1 + f_6)^2 \frac{R_6}{R_a}\frac{T_6}{T_{5a}} = \frac{\gamma_6 M_6^2}{\gamma_{5a}M_{5a}^2}\left(\frac{1 + \gamma_{5a}M_{5a}^2}{1 + \gamma_6 M_6^2}\right)^2\left(\frac{1 + \frac{\gamma_6 - 1}{2}M_6^2}{1 + \frac{\gamma_{5a} - 1}{2}M_{5a}^2}\right) \tag{B31}$$

were solved graphically with the aid of plots of Y and Z against M for constant γ where

$$Y = \frac{\gamma M^2\left[1 + \left(\frac{\gamma - 1}{2}\right)M^2\right]}{(1 + \gamma M^2)^2} \tag{B32}$$

and

$$Z = \frac{\left(1 + \frac{\gamma - 1}{2}M^2\right)^{\frac{\gamma}{\gamma - 1}}}{1 + \gamma M^2} \tag{B33}$$

[redacted]

Substituting (B32) and (B33) into (B30) and (B31) gives

$$\frac{P_6}{P_{5a}} = \frac{Z_6}{Z_{5a}} \tag{B34}$$

and

$$Y_6 = Y_{5a}\,(1 + f_6)^2\,\frac{R_6}{R_a}\,\frac{T_6}{T_5} \tag{B35}$$

The Mach number entering the primary combustor M_{5a} was read from the tables of reference 7 for calculated values of γ_{5a} and

$$\left(\frac{\rho V}{\rho_t a_t}\right)_{5a} = \frac{w_{a,6}\sqrt{\frac{R_a}{g}\,\frac{T_{5a}}{\gamma_{5a}}}}{P_2 A_{5a}} \tag{B36}$$

The value of combustor flow area A_{5a} is a design constant for each engine (cf. table I).

In calculating total-pressure ratio across the hot side of the heat exchanger, the effects of friction and cooling were separated. The total-pressure ratio due to friction was calculated from

$$\left(\frac{P_7}{P_6}\right)_{fr} = 1.0 - \frac{\gamma_6 S_{6-7}}{2A_{fl,6-7}}\,C_{fr,6-7}M_6^2\left(1 + \frac{\gamma_6 - 1}{2}\,M_6^2\right)^{\frac{-\gamma_6}{\gamma_6 - 1}} \tag{B37}$$

where $C_{fr,6-7}$ was read from the appropriate curve in reference 3 for the hot-side Reynolds number Re_{6-7} (cf. eq. (B19)). M_6 was found in the same manner as M_{5a}.

The total-pressure ratio due to cooling $(P_7/P_6)_{cl}$ was calculated in the same manner as the total-pressure ratio across the combustor. The inlet Mach number for the cooling calculation was computed from

$$M_{in} = \frac{M_6}{(P_7/P_6)_{fr}} \tag{B38}$$

The total pressure downstream of the bypass-duct throttle, P_{7a}, was calculated from the condition of constant static pressure where the flows of air and fuel-rich products mix. Static pressure at the mixing station was calculated from

[redacted]

$$p_{7a} = p_7 = P_7\left(1 + \frac{\gamma_7 - 1}{2} M_7^2\right)^{\frac{-\gamma_7}{\gamma_7 - 1}} \tag{B39}$$

where M_7 was found in the same manner as M_{5a}. At the mixing station, the flow areas assigned to the air and the fuel-rich products are design constants for each engine (cf. table I). The static-to-total-pressure ratio $(p/P)_{7a}$ was read from the tables of reference 8 for the calculated values of γ_{7a} and the static-pressure parameter

$$\frac{p_{7a} A_{7a}}{w_{7a}\sqrt{\frac{R_a T_2}{g}}}$$

The total pressure downstream of the bypass-duct throttle is

$$P_{7a} = \frac{p_{7a}}{(p/P)_{7a}} \tag{B40}$$

In order to find the total pressure at the exhaust-nozzle inlet P_8, the flow from the mixing station through the afterburner to the exhaust-nozzle inlet was approximated by a constant-area, constant-total-momentum process. Friction loss was assumed to be equal to the weight-flow-averaged dynamic pressure at station 7. The total momentum at station 8 was calculated from

$$\left(\frac{w}{g} V + pA\right)_8 = \left(\frac{\frac{w}{g} V + pA}{w\sqrt{\frac{RT}{g}}}\right)_{7a} \left(w\sqrt{\frac{RT}{g}}\right)_{7a} + \left(\frac{\frac{w}{g} V + pA}{w\sqrt{\frac{RT}{g}}}\right)_7 \left(w\sqrt{\frac{RT}{g}}\right)_7 \tag{B41}$$

The total-momentum parameter at 7a was read from the tables of reference 8 for the calculated values of γ_{7a} and $(p/P)_{7a}$. Before the total-momentum parameter at 7 could be read from the tables of reference 8, the value of $(p/P)_7$ was read from the tables of reference 7 for the known value of M_7. The values of w_8, R_8 and γ_8 needed to compute the total-momentum parameter could not be calculated until the fuel-air ratio at station 8 was calculated from

$$f_8 = \frac{1}{\eta_{AB}}\left[\frac{H_{a,8} + \left(\frac{b}{1-b}\right)H_{a,2} - \left(\frac{1}{1-b}\right)H_{a,1}}{(\overline{H} + H_{f,3}) - H_{a,8} - \psi(h)_{st,8}}\right] \tag{B42}$$

[redacted]

The value of total-pressure parameter at station 8 is read from the tables of reference 8 for the computed values of γ_8 and the total-momentum parameter at 8. Total pressure at the exhaust-nozzle inlet is

$$P_8 = \left(\frac{PA}{w\sqrt{\frac{RT}{g}}}\right)_8 \frac{w_1(1 - b)(1 + f_8)\sqrt{\frac{R_8T_8}{g}}}{A_8} \tag{B43}$$

The exhaust-nozzle-throat area for each operating point was computed from

$$A_9 = \frac{w_1(1 - b)(1 + f_8)\sqrt{\frac{R_8T_8}{\gamma_8 g}}\left(\frac{\gamma_8 + 1}{2}\right)^{\frac{\gamma_8+1}{2(\gamma_8-1)}}}{P_8} \tag{B44}$$

[redacted]

APPENDIX C

CALCULATION OF PERFORMANCE

At each flight condition the thrust parameter $C_F M_0^2$ and the specific fuel consumption sfc were calculated from

$$C_F M_0^2 = (C_{10} - C_0 - C_D)\, M_0^2 \tag{C1}$$

and

$$\text{sfc} = \frac{3600\, f_8 w_1\, (1 - b)}{C_F q_0 A_C} \tag{C2}$$

The coefficient C_{10} is defined by

$$C_{10} = \frac{1}{q_0 A_C}\left(\frac{w_8}{g} V_{10,id} C_f + \frac{w_b}{g} V_b\right) \tag{C3}$$

The ideal jet velocity is calculated from

$$V_{10,id} = \sqrt{2gJ(H_8 - h_{s,0})} \tag{C4}$$

where values of H_8 and $h_{s,0}$ are found from the known values of T_8, f_8, R_8, and P_8/p_0 and from the tables of reference 5. The nozzle thrust coefficient C_f was read from exhaust-nozzle performance curves for the known values of P_8/p_0, M_0, and A_{10}/A_9. The jet velocity of the bleed air was calculated from

$$V_b = (2gJc_{p,2}T_2)^{1/2}\left[1 - \left(\frac{p}{P}\right)_b^{\frac{\gamma_2 - 1}{\gamma_2}}\right]^{1/2} \tag{C5}$$

where

$$\left(\frac{p}{P}\right)_b = \frac{p_0}{P_2}\left(\frac{\gamma_2 + 1}{2}\right)^{\frac{\gamma_2}{\gamma_2 - 1}} \tag{C6}$$

[redacted]

The critical pressure ratio is included in equation (C6) to account for all losses incurred in obtaining thrust from the bleed air. The coefficient C_O is defined by

$$C_O = \frac{w_1 V_O}{g q_O A_C} = \frac{2 w_1 a_O}{g \gamma_O p_O M_O A_C} \tag{C7}$$

The total-drag coefficient is defined by

$$C_D = \frac{A_l}{A_C} \left(C_{D,a} + C_{D,b} + C_{D,c} + C_{D,n} \right) \tag{C8}$$

The additive-, bleed-, and cowl-pressure-drag coefficients were read from the inlet performance curves (fig. 2), while the nacelle-drag coefficient was read from curves based on the pressure-drag coefficients of slender conical bodies (ref. 9) and the equation for turbulent-skin-friction coefficient.

$$C_{fr} = \frac{0.0306K}{(Re)^{1/7} \left(1 + \frac{\gamma_O - 1}{4} M_O^2 \right)^{5/7}} \tag{C9}$$

where $K = 1.0$ and $\gamma_O = 1.4$.

[redacted]

REFERENCES

1. Hausmann, George F.: Study of SF-1 Propulsion Systems for Flight at High Altitudes and Mach Numbers. Pt. I - Summary Report. TR 57-55, WADC, Mar. 1957.

2. Lieblein, Seymour, Lewis, George W., Jr., and Sandercock, Donald M.: Experimental Investigation of an Axial-Flow Compressor Inlet Stage Operating at Transonic Relative Inlet Mach Numbers. I - Over-All Performance of Stage with Transonic Rotor and Subsonic Stators up to Relative Inlet Mach Number of 1.1. NACA RM E52A24, 1952.

3. Kays, W. M., and London, A. L.: Compact Heat Exchangers. The National Press, Palo Alto (Calif.), 1955.

4. English, Robert E., and Wachtl, William W.: Charts of Thermodynamic Properties of Air and Combustion Products from 300° to 3500° R. NACA TN 2071, 1950.

5. Hall, Eldon W., and Weber, Richard J.: Tables and Charts for Thermodynamic Calculations Involving Air and Fuels Containing Boron, Carbon, Hydrogen, and Oxygen. NACA RM E56B27, 1956.

6. Reynolds, Thaine W.: Heat-Exchanger-Core Weights for Use With Hydrogen-Expansion Turbine. NACA RM E57H09, 1957.

7. Lewis Laboratory Computing Staff: Tables of Various Mach Number Functions for Specific-Heat Ratios from 1.28 to 1.38. NACA TN 3981, 1957.

8. Turner, L. Richard, Addie, Albert N., and Zimmerman, Richard H.: Charts for the Analysis of One-Dimensional Steady Compressible Flow. NACA TN 1419, 1948.

9. Fraenkel, L. E.: The Theoretical Wave Drag of Some Bodies of Revolution. Rep. No. Aero. 2420, British RAE, May 1951.

[redacted]

TABLE I. - DESIGN CONSTANTS FOR HYDROGEN EXPANSION ENGINES

Design constants	Number of compressor stages		
	1	2	3
Compressor total-pressure ratio at sea-level takeoff	1.455	1.830	2.315
Fraction of compressor airflow bled to cool afterburner, b	.07	.07	.07
Turbine flow parameter, $(w\sqrt{T}/P)_4$, sq ft $(^{\circ}R)^{1/2}/sec$	.0001185	.000272	.000300
Heat-exchanger surface (ref. 3)	S-2.00 -1.00	S-2.00 -1.00	S-2.00 -1.00
Hydraulic diameter of hot side, $D_{h,6-7}$, ft	.0327	.0327	.0327
Free-flow area of hot side, $A_{fl,6-7}$, sq ft	.5552	.7315	.7161
Hydraulic diameter of cold side, $D_{h,3-4}$, ft	.0291	.0291	.0291
Free-flow area of cold side, $A_{fl,3-4}$, sq ft	.009224	.01535	.00621
Heat-transfer surface area of hot side, S_{6-7}, sq ft	14.91	22.22	25.23
Cold-side to hot-side surface area ratio, S_{3-4}/S_{6-7}	.931	.931	.931
Primary-combustor flow area, A_{5a}, sq ft	.348	.600	.600
Flow area for fuel-rich products at mixing station, A_7, sq ft	.47	1.46	1.10
Flow area for bypassed air at mixing station, A_{7a}, sq ft	3.175	2.60	2.50
Flow area of afterburner, A_8, sq ft	3.645	4.06	3.60
Compressor frontal area, A_C, sq ft	1.00	1.00	1.00
Inlet-lip area, A_1, sq ft	2.266	2.266	2.266
Exhaust-nozzle-exit area, A_{10}, sq ft	5.186	5.177	5.263
Nacelle-length to exit-diameter ratio	1.983	1.985	1.969
Compressor equivalent specific weight flow at sea-level takeoff, $w_1\sqrt{\theta_1}/\delta_1 A_C$, lb/(sec)(sq ft)	32.52	32.52	32.52

[redacted]

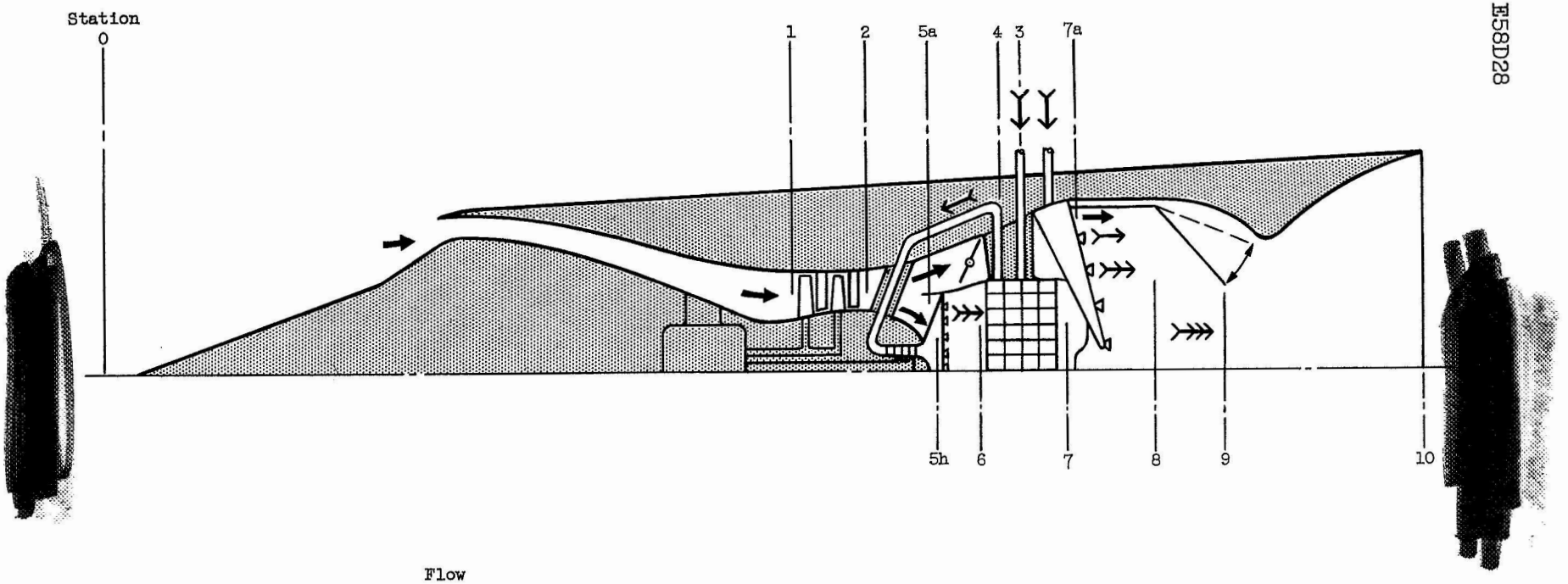

Figure 1. - Hydrogen expansion engine.

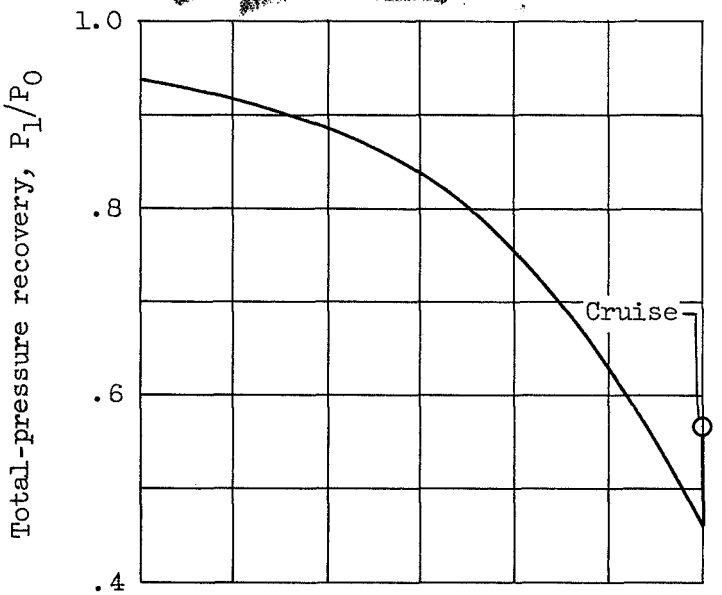

(a) Recovery.

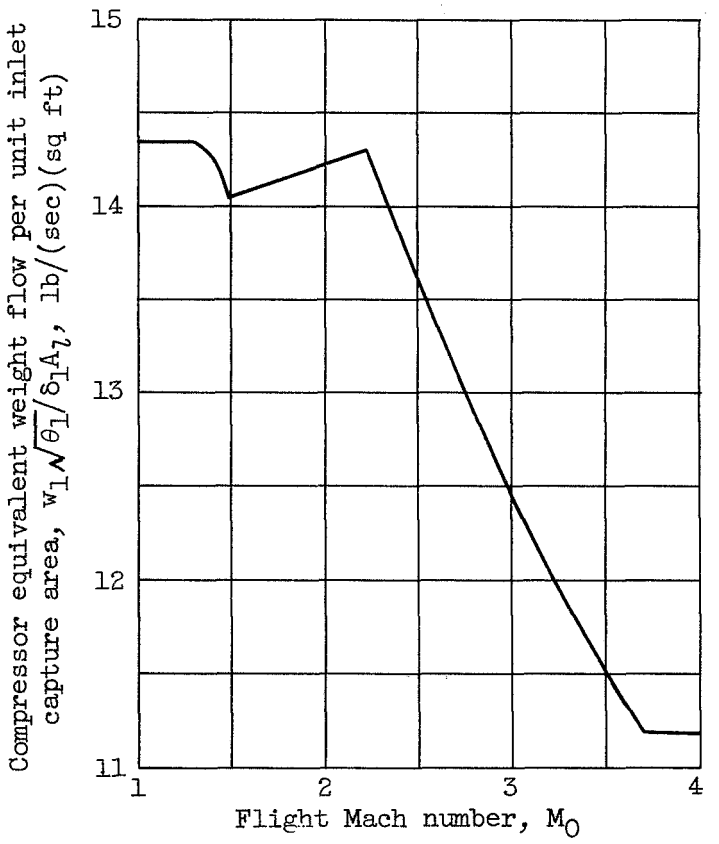

(b) Flow.

Figure 2. - Inlet performance.

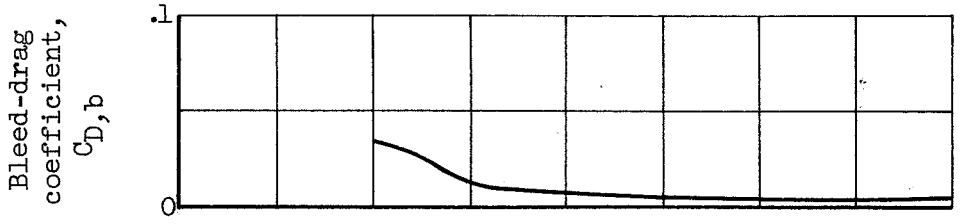

(c) Bleed drag.

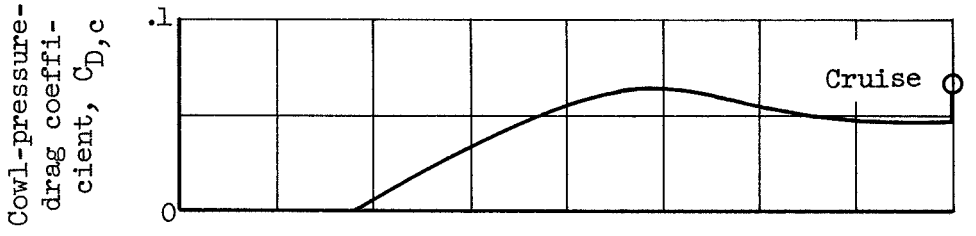

(d) Cowl drag.

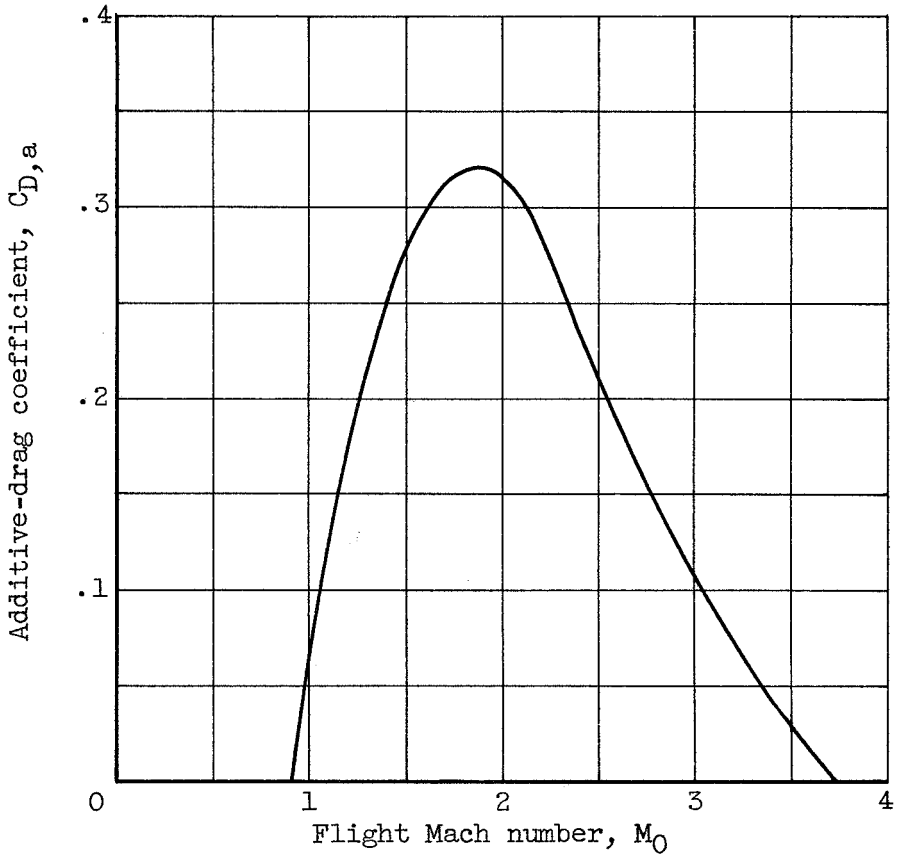

(e) Additive drag.

Figure 2. - Concluded. Inlet performance.

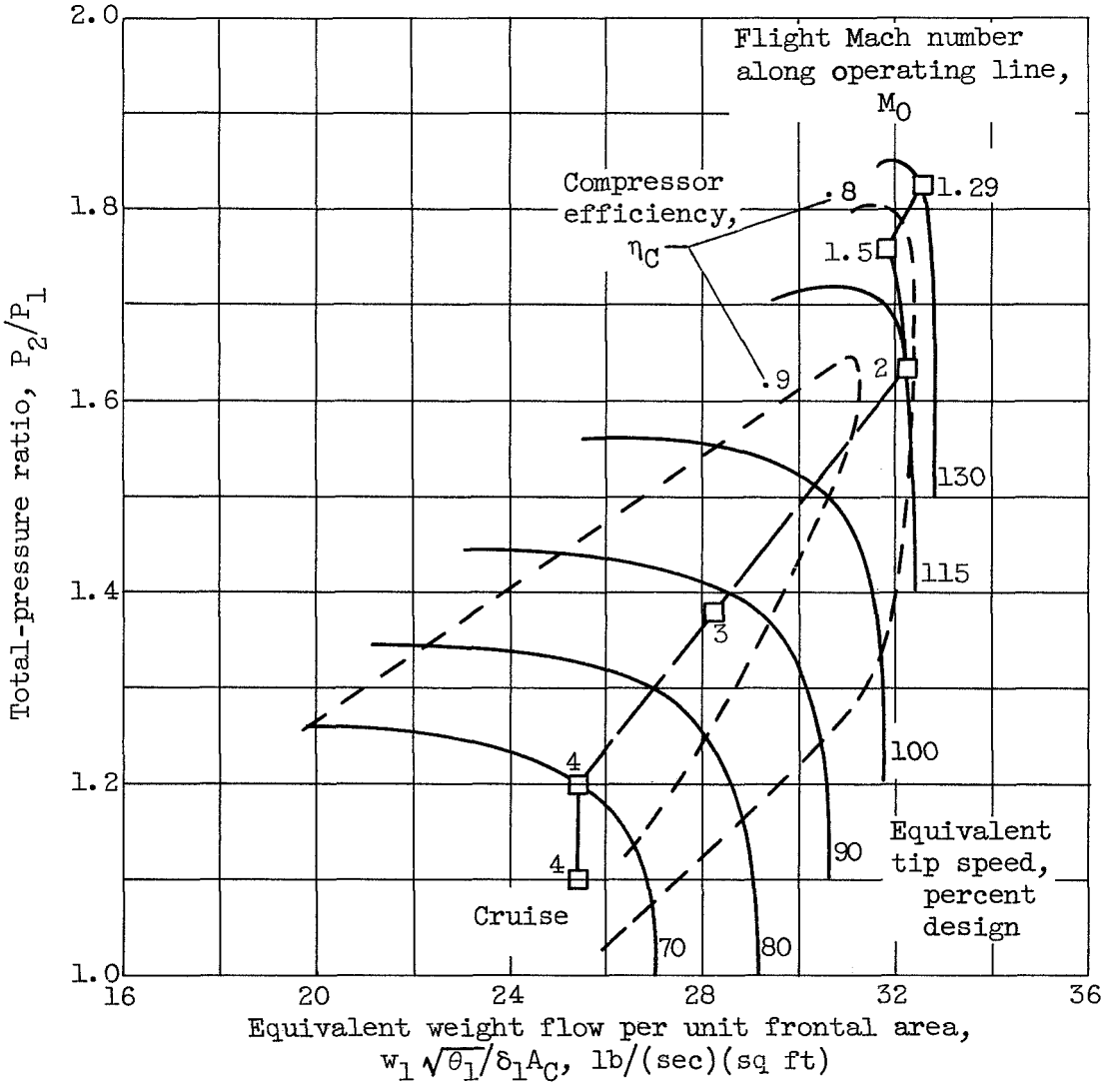

Figure 3. - Operating line on two-stage-compressor performance map.

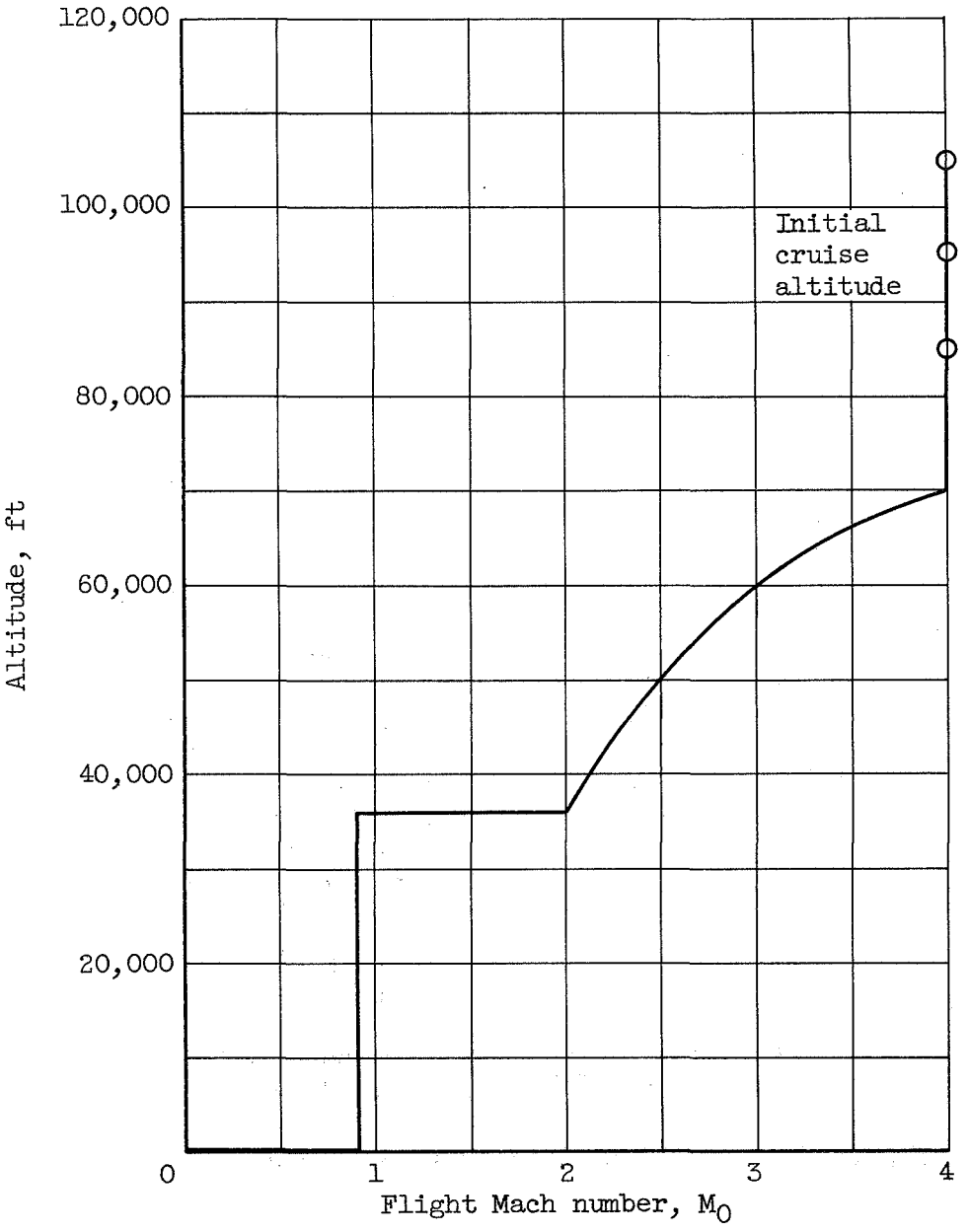

Figure 4. - Flight path.

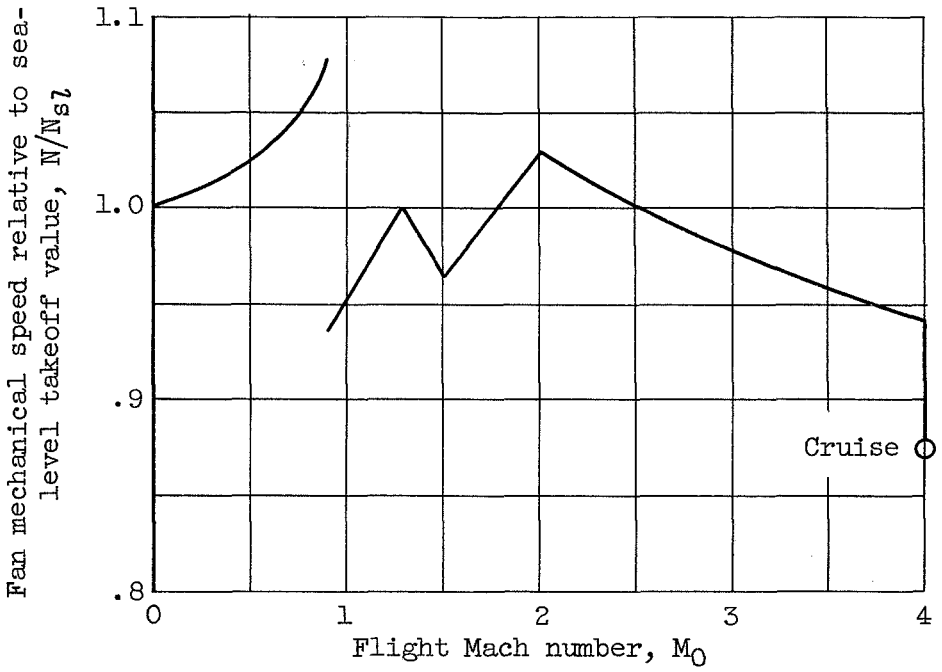

Figure 5. - Mechanical-speed variation of two-stage fan for assigned operating schedule. Initial cruise altitude, 85,000 feet.

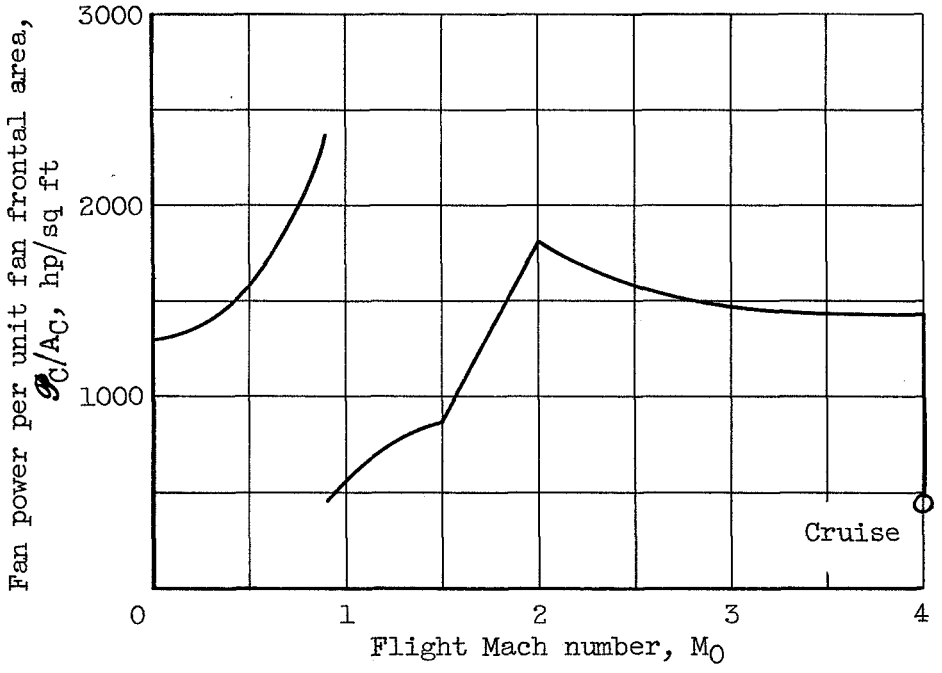

Figure 6. - Power variation of two-stage fan for assigned operating schedule. Initial cruise altitude, 85,000 feet.

[redacted]

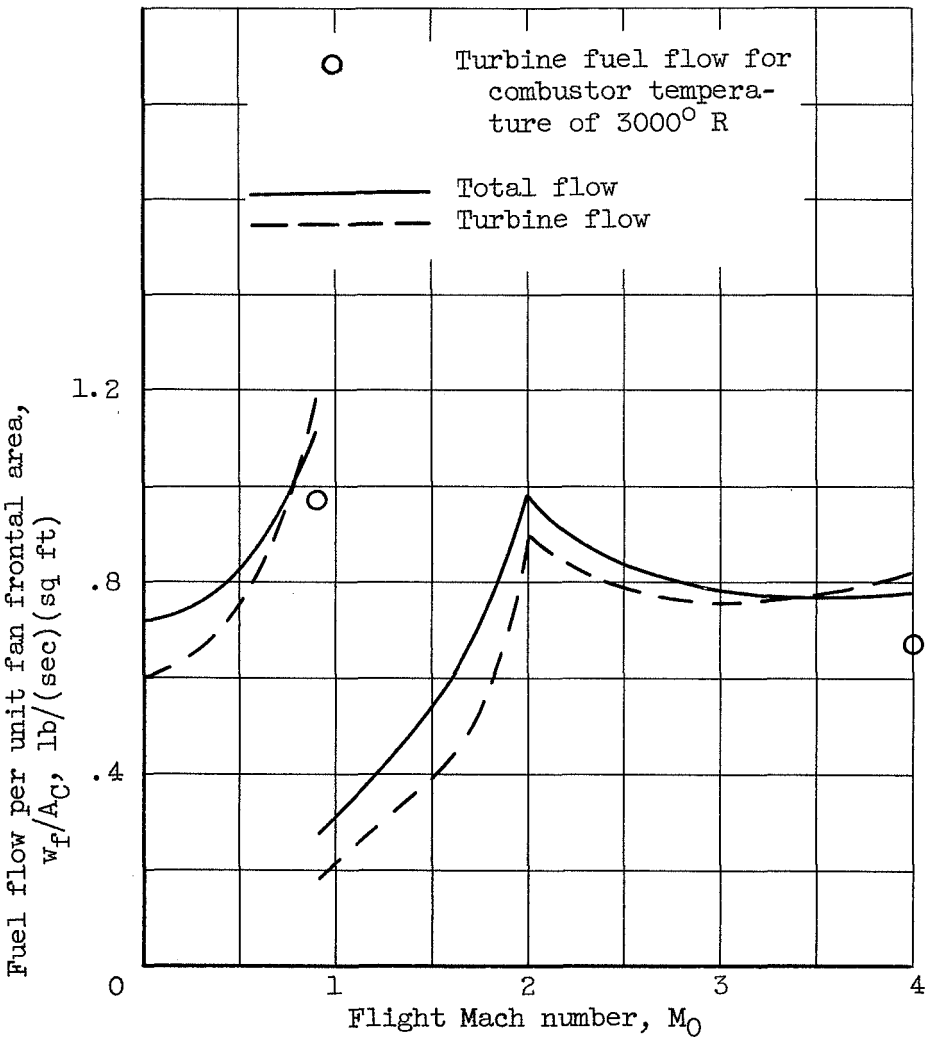

Figure 7. - Fuel-flow requirements for assigned operating schedule. Engine with two-stage compressor; combustor temperature, 2500° R; afterburner temperature, 4000° R.

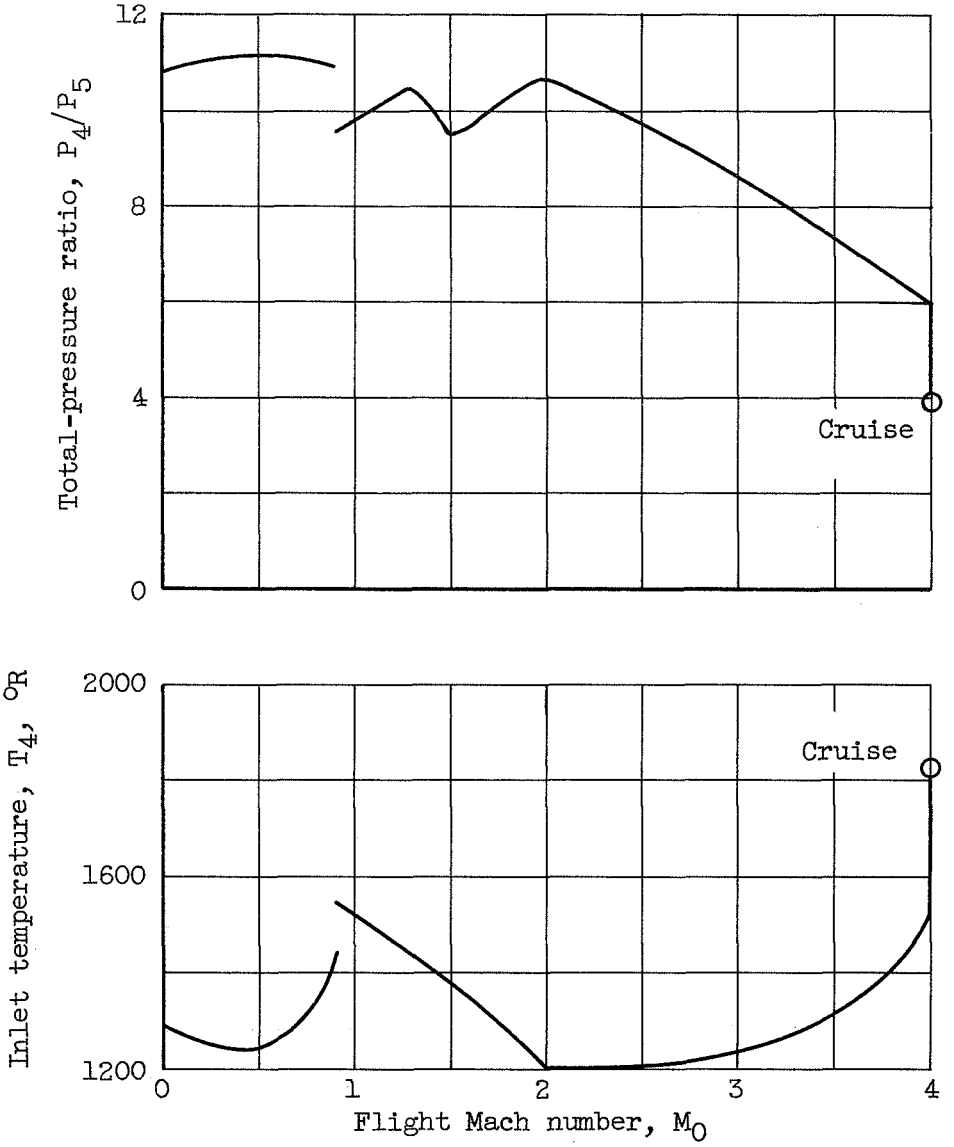

Figure 8. - Turbine-inlet-temperature and total-pressure-ratio variations for assigned operating schedule. Engine with two-stage compressor; initial cruise at 85,000-foot altitude and 3500° R afterburner temperature.

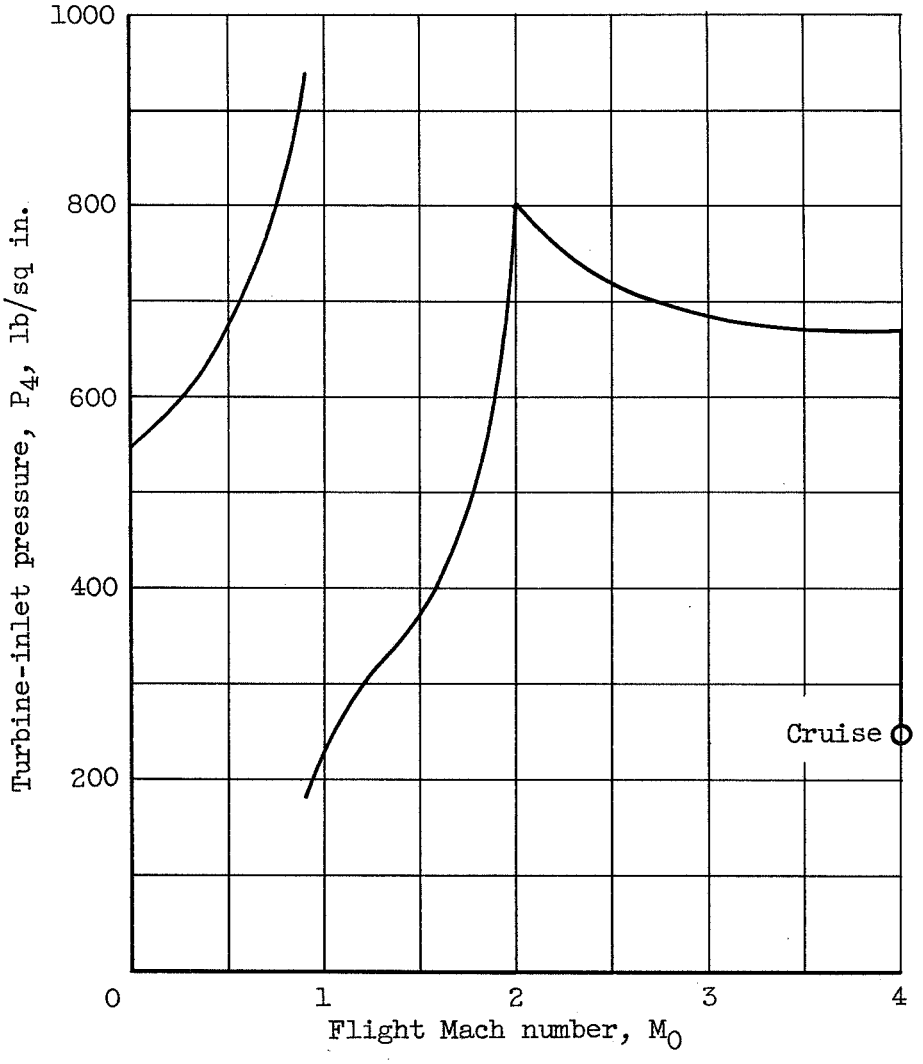

Figure 9. - Turbine-inlet-pressure variation for assigned operating schedule. Engine with two-stage compressor; initial cruise at 85,000-foot altitude and 3500° R afterburner temperature.

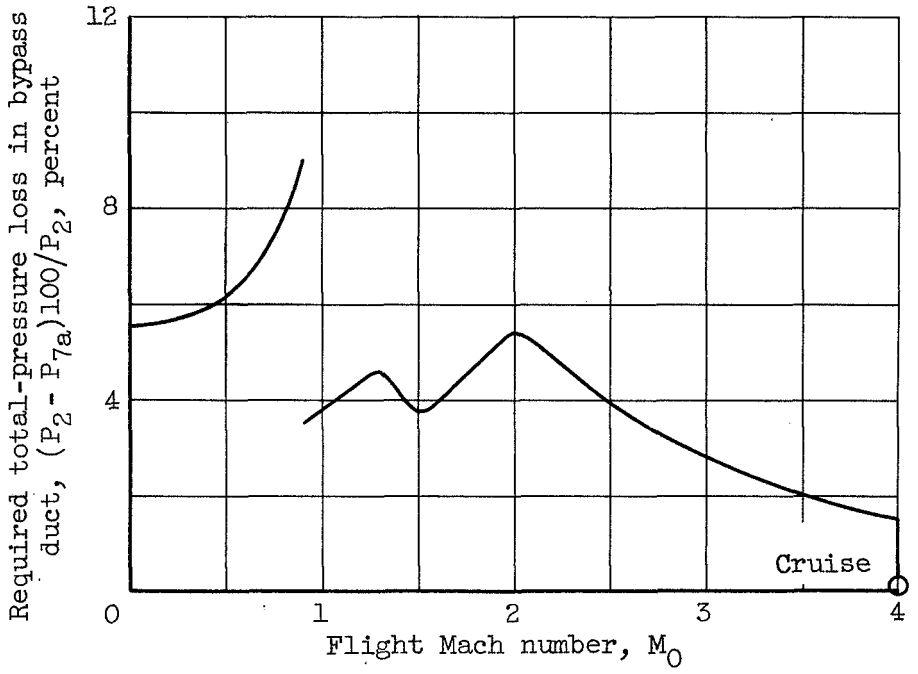

Figure 10. - Required total-pressure loss in bypass duct for assigned operating schedule. Engine with two-stage compressor; initial cruise at 85,000-foot altitude and 3500° R afterburner temperature.

[redacted]

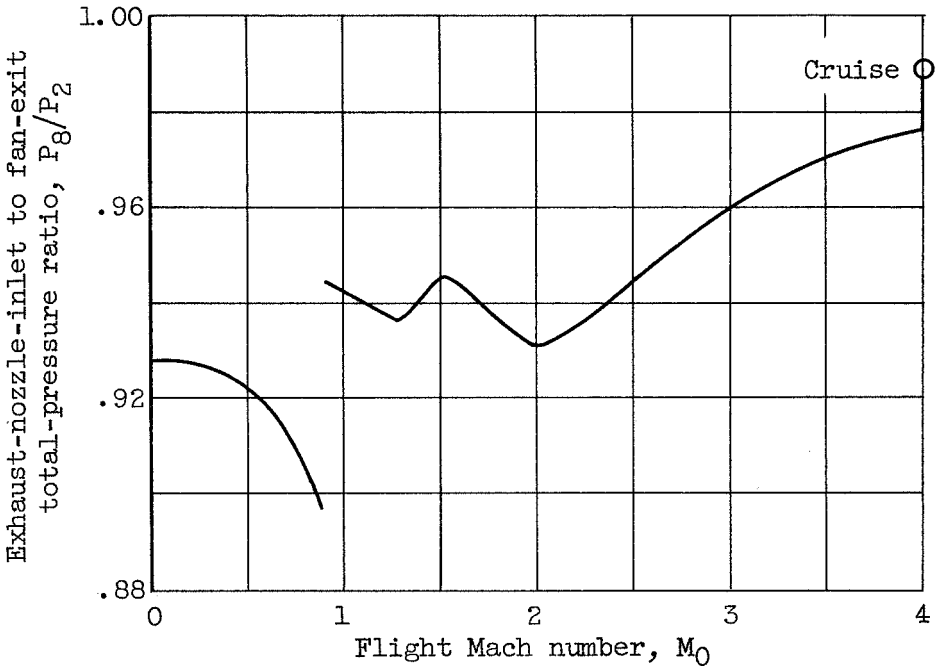

Figure 11. - Total-pressure losses from fan exit to exhaust-nozzle inlet for assigned operating schedule. Engine with two-stage compressor; initial cruise at 85,000-foot altitude and 3500° R afterburner temperature.

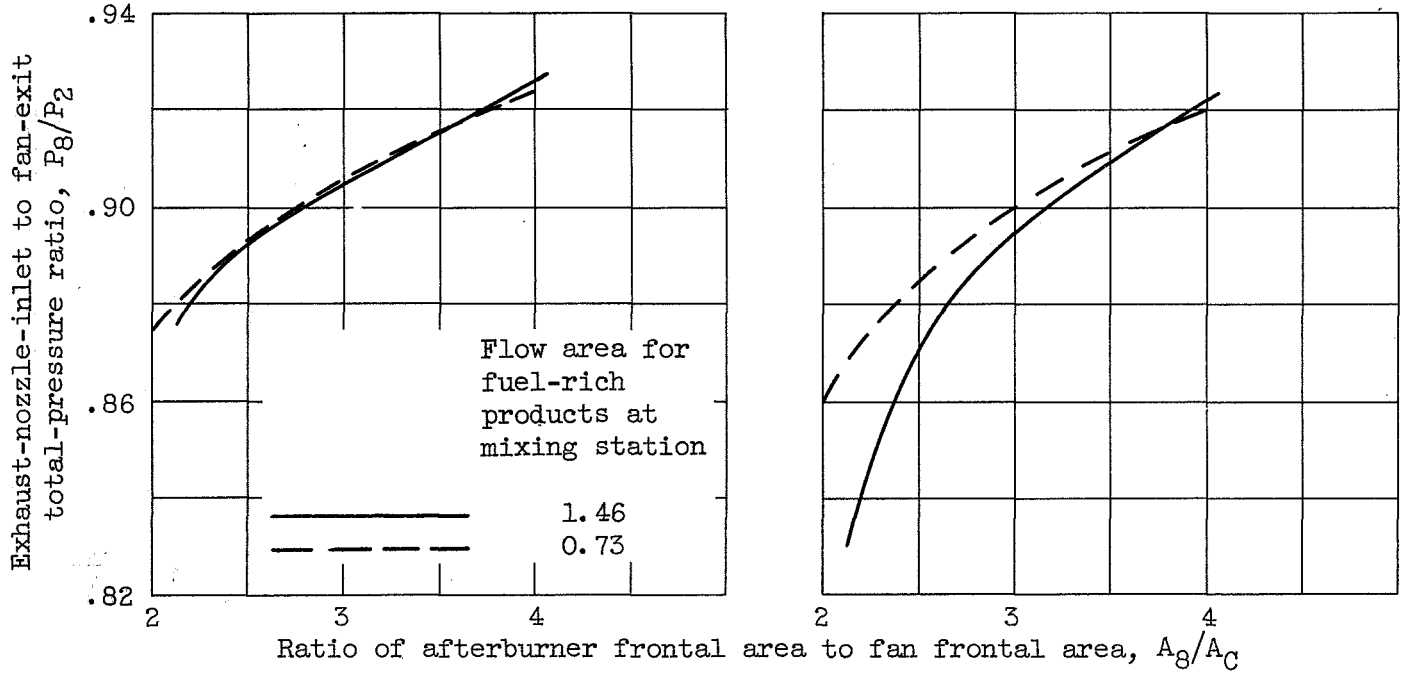

(a) One "q" friction loss.

(b) Two "q" friction loss.

Figure 12. - Effect of afterburner frontal area, friction, and flow area for fuel-rich products at mixing station on engine total-pressure losses. Engine with two-stage compressor; Mach 0 and sea level.

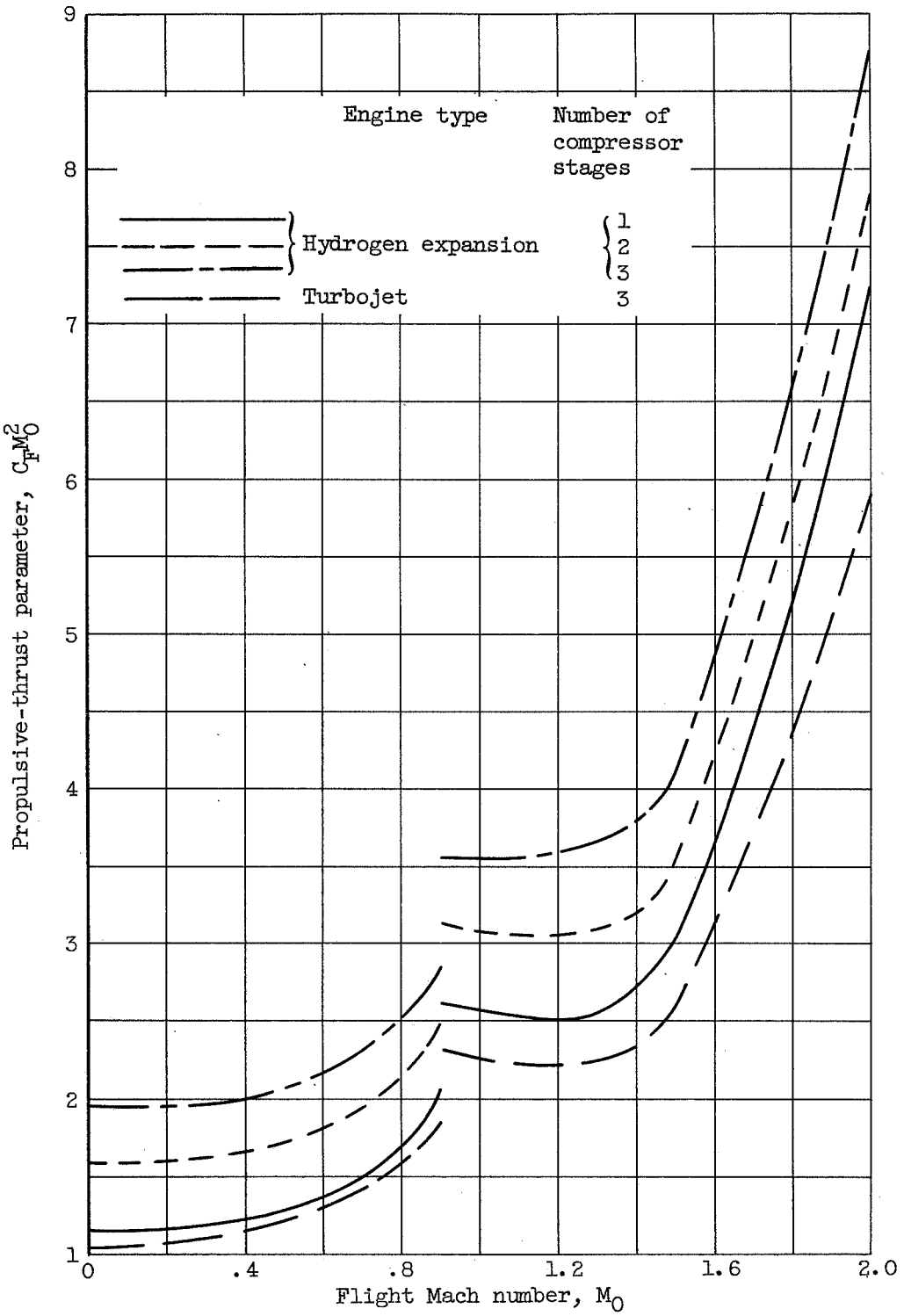

(a) Thrust variation from Mach 0 to 2.0.

Figure 13. - Engine performance during acceleration and climb.

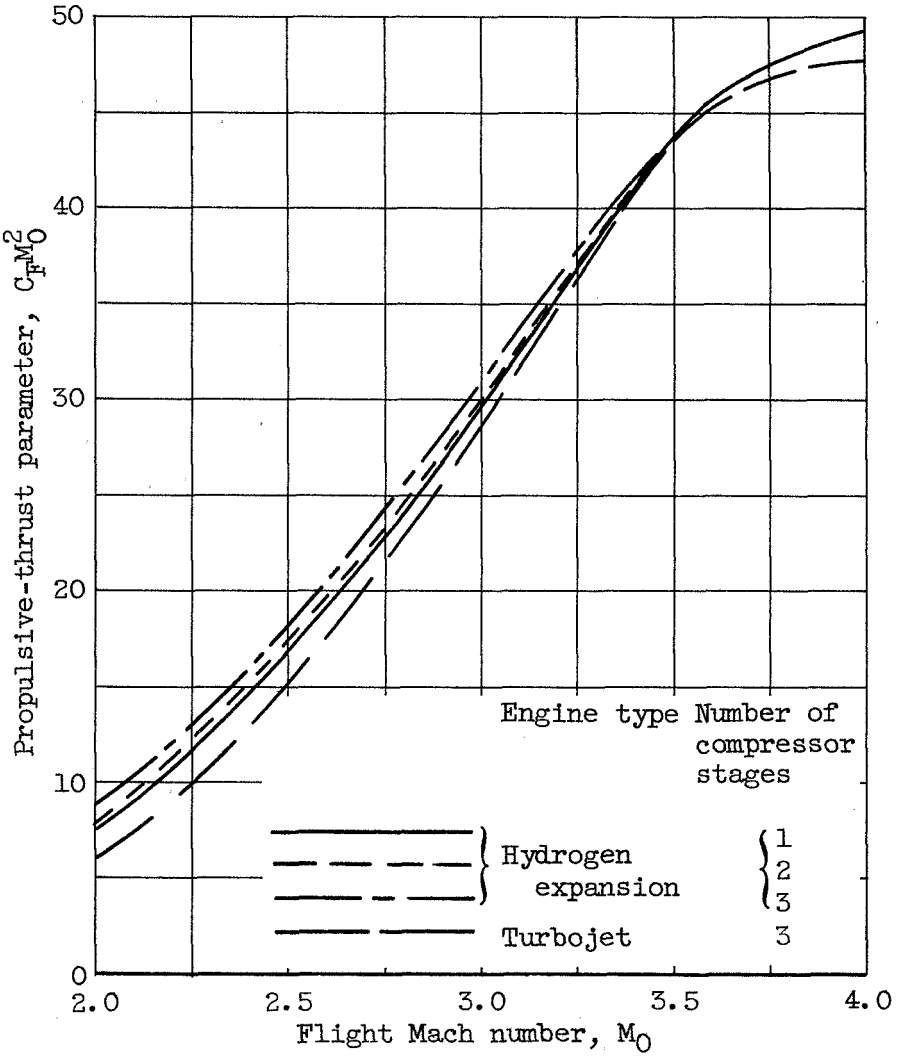

(b) Thrust variation from Mach 2 to 4.

Figure 13. - Continued. Engine performance during acceleration and climb.

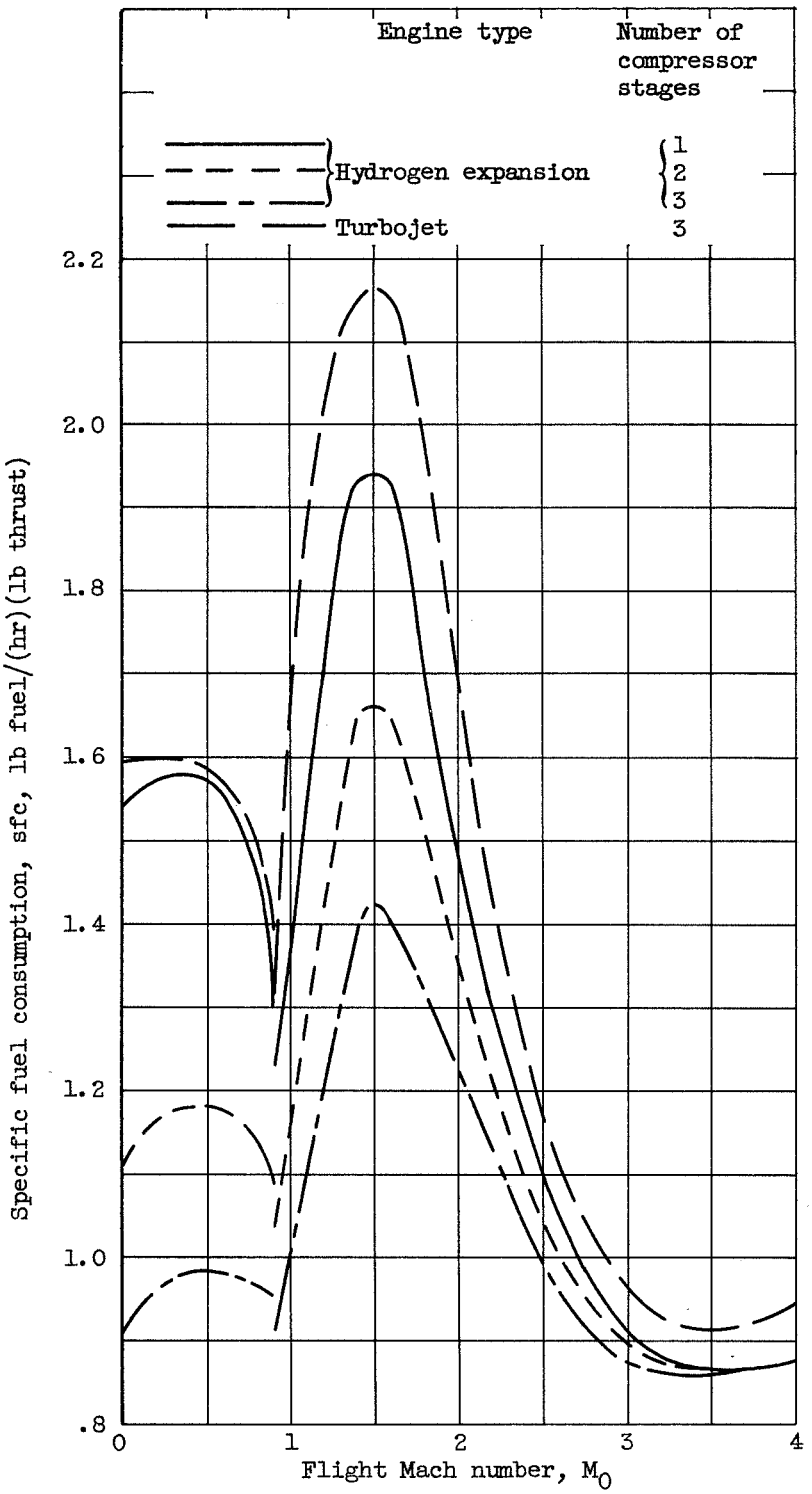

(c) Specific-fuel-consumption variation.

Figure 13. - Continued. Engine performance during acceleration and climb.

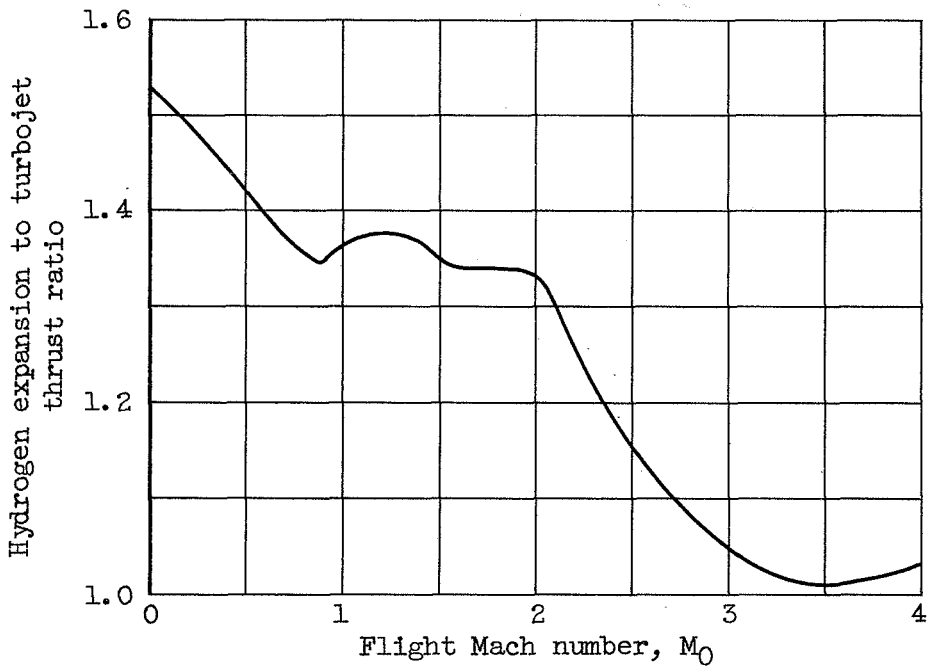

(d) Relative performance of hydrogen expansion engine with two-stage compressor and turbojet engine with three-stage compressor.

Figure 13. - Concluded. Engine performance during acceleration and climb.

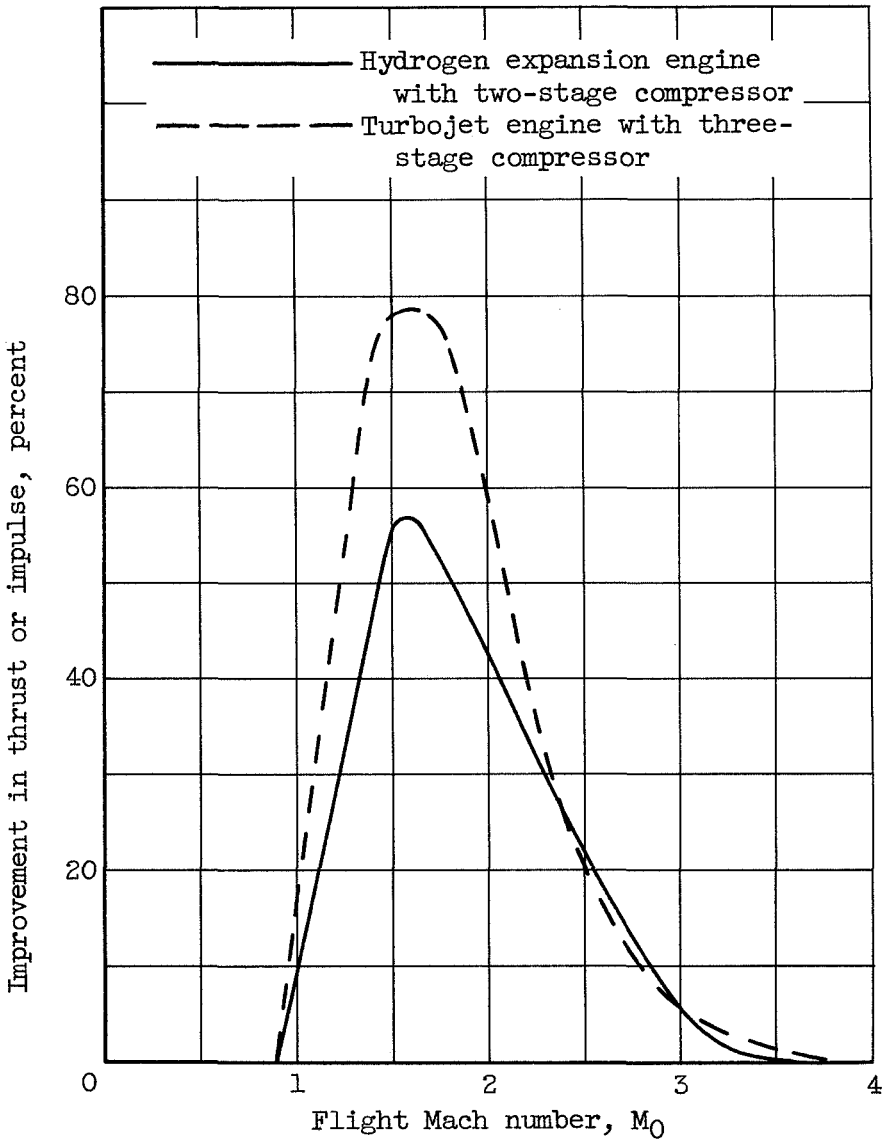

Figure 14. - Improvement in performance during acceleration and climb by using variable inlet and exhaust nozzle.

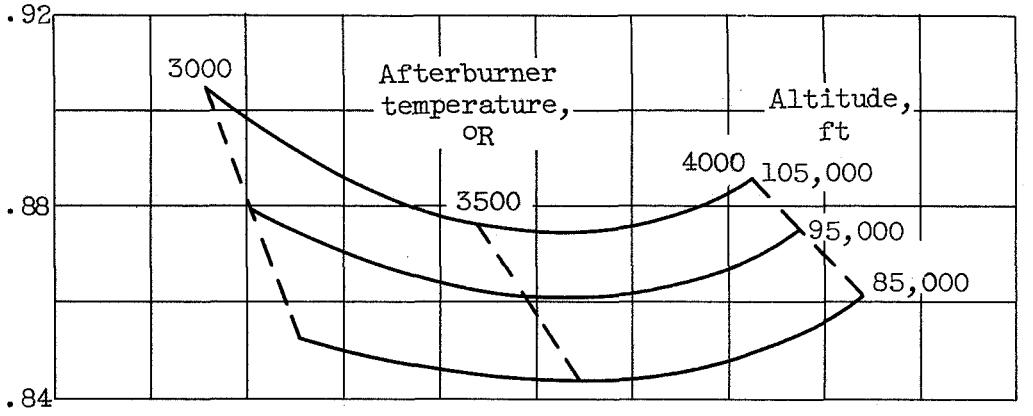

(a) Hydrogen expansion engine with three-stage compressor.

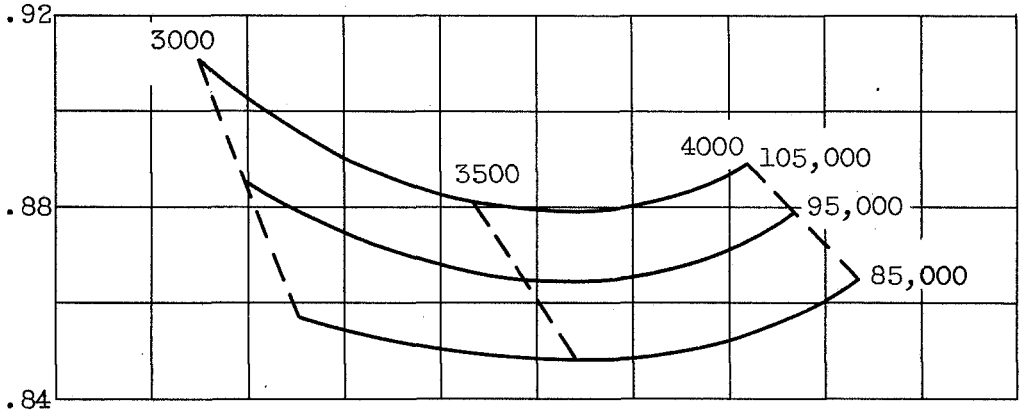

(b) Hydrogen expansion engine with two-stage compressor.

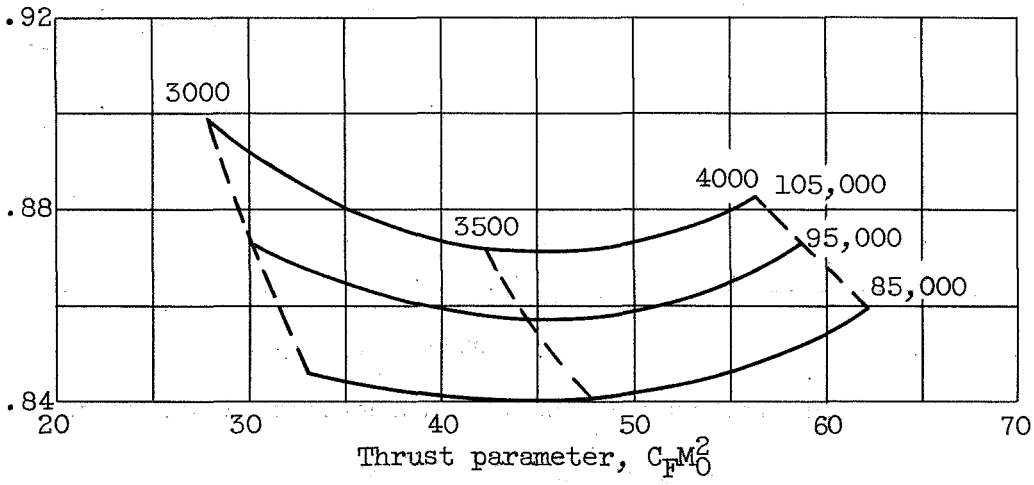

(c) Hydrogen expansion engine with one-stage compressor.

Specific fuel consumption, sfc, lb fuel/(hr)(lb thrust)

Figure 15. - Effect of afterburner temperature and altitude on cruise performance at Mach 4.0.

4881

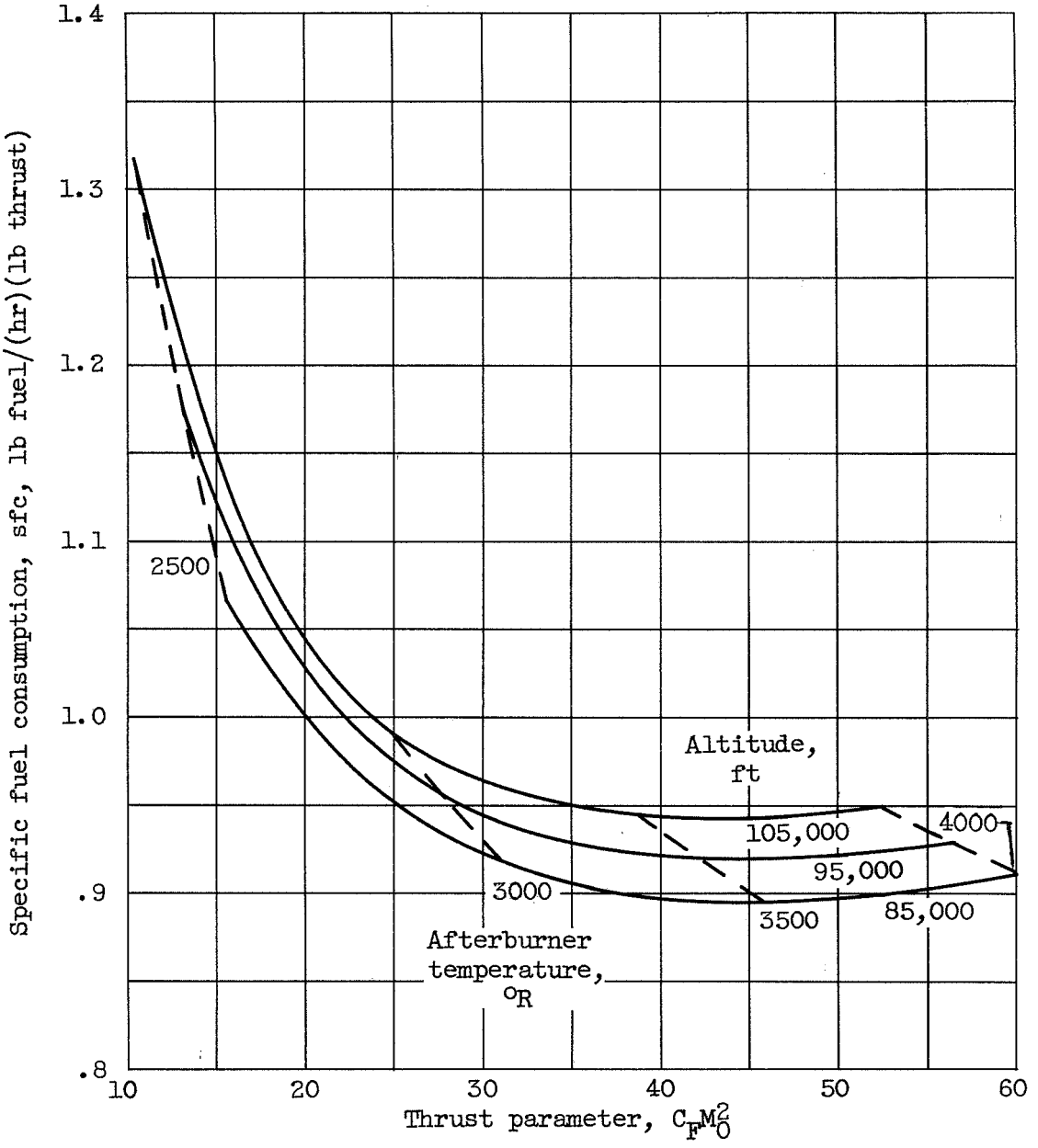

(d) Turbojet engine with three-stage compressor.

Figure 15. - Concluded. Effect of afterburner temperature and altitude on cruise performance at Mach 4.0.

[redacted]